Energy 150 (2018) 1039–1057

Contents lists available at ScienceDirect

Energy

journal homepage: www.elsevier.com/locate/energy

Multiobjective economic-environmental power dispatch with stochastic wind-solar-small hydro power

Partha P. Biswas [a, *], P.N. Suganthan [a], B.Y. Qu [b], Gehan A.J. Amaratunga [c]

[a] School of Electrical and Electronic Engineering, Nanyang Technological University, Singapore
[b] School of Electrical and Information Engineering, Zhongyuan University of Technology, China
[c] Department of Engineering, University of Cambridge, UK

ARTICLE INFO

Article history:
Received 25 July 2017
Received in revised form
26 February 2018
Accepted 1 March 2018
Available online 3 March 2018

Keywords:
Economic-environmental dispatch
Wind power generator
Solar photovoltaic
Small-hydro power unit
Uncertainty modelling
Multiobjective evolutionary algorithms

ABSTRACT

Economic-environmental power dispatch is one of the most popular bi-objective non-linear optimization problems in power system. Classical economic power dispatch problem is formulated with only thermal generators often ignoring security constraints of the network. But importance of reduction in emission is paramount from environmental sustainability perspective and hence penetration of more and more renewable sources into the electrical grid is encouraged. However, most common forms of renewable sources are intermittent and uncertain. This paper proposes multiobjective economic emission power dispatch problem formulation and solution incorporating stochastic wind, solar and small-hydro (run-of-river) power. Weibull, lognormal and Gumbel probability density functions are used to calculate available wind, solar and small-hydro power respectively. Some conventional generators of the standard IEEE 30-bus system are replaced with renewable power sources for study purpose. Network security constraints such as transmission line capacities and bus voltage limits are also taken into consideration alongwith constraints on generator capabilities and prohibited operating zones for the thermal units. Decomposition based multiobjective evolutionary algorithm and summation based multiobjective differential evolution algorithm are applied to the problem under study. An advanced constraint handling technique, superiority of feasible solutions, is integrated with both the multi-objective algorithms to comply with system constraints. The simulation results of both the algorithms are summarized, analyzed and compared in this study.

1. Introduction

Economic-environmental dispatch (EED), also termed as economic-emission dispatch, has two aspects of consideration. Economic dispatch (ED) deals with economic consideration of generation units in a power system. Optimization on this front aims to minimize generation or fuel cost by optimal scheduling of generators to mitigate certain load demand in a specified interval. Emission objective performs similar task of scheduling generation units with target of minimizing volume of greenhouse gases that emanate from conventional thermal power generators. Classical single objective ED problem considers only economic aspect of power dispatch. However, due to environmental regulation and carbon tax imposition in many countries, more importance is exercised on controlling emission. Thus, formulation of optimization problem with both the objectives of cost and emission becomes necessary so that a compromised solution can be obtained. Irrespective of the number of objectives for power dispatch problem, all constraints pertaining to generator capacity, network operation and security are to be satisfied.

In recent times, several literature studied single objective ED problem applying evolutionary algorithms. Adarsh et al. [1] implemented chaotic bat algorithm (CBA) to perform the optimization. A new hybrid grey wolf optimizer (HWGO) with addition of mutation and crossover operators into grey wolf optimizer was proposed in Ref. [2] to solve the same single objective ED problem. Multi-fuel option and valve-point loading effect of steam turbine generators were introduced in Ref. [3] in solving ED problem. Delshad et al. [4] performed the study using backtracking search algorithm (BSA) with added complexity of generator prohibited

* Corresponding author.
E-mail addresses: parthapr001@e.ntu.edu.sg (P.P. Biswas), epnsugan@ntu.edu.sg (P.N. Suganthan), qby1984@hotmail.com (B.Y. Qu), gaja1@hermes.cam.ac.uk (G.A.J. Amaratunga).

https://doi.org/10.1016/j.energy.2018.03.002
0360-5442/

Nomenclature

Abbreviations

EED	economic-environmental dispatch
MOEA/D	multiobjective evolutionary algorithm based on decomposition
SMODE	summation based multiobjective differential evolution
SF	superiority of feasible solutions
TG	thermal power generator
WG	wind generator
PV	photovoltaic
SPH	a solar PV and a small-hydro (run-of-river) power unit
ISO	independent system operator
PDF	probability density function
POZ	prohibited operating zone

Symbol

P_{TGi}	power output from the i-th thermal generator
P_{ws}	scheduled power from the wind power plant
P_{ss}	scheduled power from the solar PV plant
P_{ssh}	scheduled power from the combined solar PV and small-hydro unit
P_{wav}	actual available power from the wind power plant
P_{sav}	actual available power from the solar PV plant
P_{shav}	actual available power from the combined solar PV and small-hydro unit
g_w	direct cost coefficient for the wind power
h_s	direct cost coefficient for the solar PV power
m_h	direct cost coefficient for the small-hydro unit power
K_{Rw}	reserve cost coefficient for overestimation of wind power
K_{Pw}	penalty cost coefficient for underestimation of wind power
K_{Rs}	reserve cost coefficient for over-estimation of solar power
K_{Ps}	penalty cost coefficient for under-estimation of solar power
K_{Rsh}	reserve cost coefficient for combined solar and hydro system
K_{Psh}	penalty cost coefficient for combined solar and hydro system
G_s	solar irradiance in W/m^2
Q_w	river flow rate in m^3/s
$f_v(v)$	probability of wind speed v
$f_G(G_s)$	probability of solar irradiance G_s
$f_Q(Q_w)$	probability of river flow rate Q_w
p_{wr}	rated output power of a wind turbine
P_{sr}	rated output power of the solar PV plant
P_{hr}	rated output power of the small-hydro unit
α, β	Weibull PDF scale and shape parameters respectively
μ, σ	lognormal PDF mean and standard deviation respectively
λ, γ	Gumbel PDF location and scale parameters respectively
P_{loss}	real power loss in the network
VD	cumulative voltage deviation of load buses in the network

operating zone (POZ) to Ref. [3]. To include emission as an objective, formulation of multiobjective EED (MOEED) was necessary. In an effort to solve MOEED problem, weighted sum approach was adopted in Ref. [5] applying modified artificial bee colony (MABC). Using classical genetic algorithm similar weighted sum approach was taken in Ref. [6]. The parameter free bare-bones multiobjective particle swarm optimization (BB-MOPSO), proposed in Ref. [7], showed improved results on MOEED than MOPSO. Rao et al. [8] introduced adaptive clonal selection algorithm for the multi-objective optimization. The MOEED problem in these literature dealt with thermal generators only. EED problem with thermal and wind energy sources had also been studied in recent years. Mondal et al. [9] added penalty cost for underestimation and reserve cost for overestimation of stochastic wind power in solving MOEED problem using gravitational search algorithm (GSA). Quantum inspired particle swarm optimization (QPSO) was used in Ref. [10] for stochastic EED with uncertain wind power and carbon tax. Total operation cost of thermal and wind generators was demonstrated with single objective model using Gbest guided artificial bee colony (GABC) in Ref. [11]. Literatures [9–11] transformed multiobjective EED problem into single objective, thereby whole set of non-dominated solutions in the multiobjective problem could not be utilized for dispatch decision making. Multiobjective evolutionary algorithms for EED problem with wind generators had been studied in a few literature. In employing non-dominated sorting genetic algorithm-II (NSGA-II) to MOEED problem, literature [12] included valve-point effect in addition to penalty and reserve costs for stochastic wind power. A practical 2m-point model was used for wind power uncertainty in Ref. [13] when applying online meta-heuristic for the MOEED problem. Qu et al. [14] adopted summation based multiobjective differential evolution (SMODE) to solve the problem where stochastic wind power was treated as a constraint. Similar approach was taken in Ref. [15] when applying multiobjective evolutionary algorithm based on decomposition (MOEA/D) coupled with penalty function method for handling system constraints. Modified teaching learning algorithm (MTLA) was applied in Ref. [16] to obtain the set of *Pareto* optimal solutions while adopting same model for wind energy as in Ref. [13]. EED with thermal-solar power was studied in Ref. [17] where in implementing particle swarm optimization (PSO) multiobjective problem was converted into single objective one.

Problem formulation and solution with thermal-wind-solar units together in power system need more research as only a few literature could be traced regarding the same. Single objective dynamic ED solutions with all these three types of sources were proposed in Ref. [18]. Reddy [19] performed optimal scheduling with thermal-wind-solar power alongwith battery storage. Biswas et al. [20] suggested an approach to solve optimal power flow problem with different probability density functions (PDFs) for wind and solar power. These studies were all for single objective optimization. Present study proposes multiobjective economic-environmental (MOEED) power dispatch problem formulation with thermal, wind, solar and small-hydro power generators. To the best of our knowledge, no literature performed even single objective ED with all these renewable sources together. For our study purpose, standard IEEE 30-bus system is adapted to include wind, solar PV and small-hydro power units. Stochastic nature of the renewable sources viz. wind, solar and small-hydro (run-of-river) power are modelled using Weibull, lognormal and Gumbel PDFs respectively. Penalty cost for underestimation and reserve cost for

overestimation of these intermittent sources are suitably added to the generation cost. The sets of *Pareto* solutions are obtained for the multiobjective problem using multiobjective evolutionary algorithm based on decomposition (MOEA/D) [21,22] and summation based multiobjective differential evolution (SMODE) [23]. Another important aspect of EED problem is compliance with system constraints. Most of the literature did not consider network security constraints in EED problem. However, load bus voltages have certain operating limits and transmission line capacities are also defined. Our research presented in this paper considers network security constraints together with constraints on generator capability and prohibited operating zones (POZs). Furthermore, many literature handled system constraints by penalty factor approach where the penalty coefficient is decided largely by trial and error method. Inconsiderate selection of penalty coefficient may lead to violation of system constraint, often without the cognizance of the designer. In present study, we adopt evolutionary algorithm compatible efficient constraint handling technique called superiority of feasible solutions (SF) [24]. Both the multiobjective evolutionary algorithms (MOEAs) employed in the study are meant for unconstrained optimization problems. SF technique is tactically entwined with these MOEAs to deal with the system constraints. The algorithms MOEA/D-SF and SMODE-SF thus implemented can successfully perform the task of multiobjective optimization conforming to system constraints. In summary, the contributions of this work can be pointwise listed as below:

- Economic-environmental dispatch (EED) problem formulation with thermal, wind, solar and small-hydro power.
- Applying appropriate probability density functions (PDFs) to model stochastic nature of all these renewable sources.
- Consideration of both network security constraints and generator prohibited operating zones (POZs) in solving EED problem.
- Integrating a proper constraint handling technique viz. superiority of feasible solutions (SF) with decomposition based multiobjective evolutionary algorithm (MOEA/D).
- Comparison of EED solutions obtained with multiple runs of both MOEA/D-SF and SMODE-SF algorithms.
- Critical analysis of results against violation of constraints in MOEED problem.

The remainder of the paper is organized in following manner. Mathematical model of MOEED problem alongwith constraints is included in section 2. Wind, solar and small-hydro power uncertainties are modelled in section 3. Section 4 elaborates the algorithms MOEA/D-SF and SMODE-SF and their application in MOEED problem. Case studies and simulation results are discussed in section 5. The paper ends with concluding remarks in section 6.

2. Mathematical models

Basic parameters of the modified IEEE 30-bus network are provided in Table 1. The single line diagram of the adapted network is depicted in Fig. 1. The network has 3 thermal generators at buses 1, 2 and 8. Output of a windfarm is connected to bus 5 while solar PV unit is supplying power to bus 11. Small-hydro power in most cases is 'run-of-river', where usually little or no storage is needed [25]. Natural flow of river to downhill is diverted by a weir and controlled water is channelized to the turbine before the water is released back to the downstream of river. Small-hydro unit can generate maximum output in the range of only few MW [25]. Hence, a solar PV unit is considered to be connected together with the small-hydro power unit at bus 13. As an obvious fact, outputs from wind, solar and small-hydro are all variables and any deficit in total output from these units must be mitigated by spinning reserve. As listed in Table 1, the network has 11 control variables that can be optimized for efficient and economical operation of the network. The control variables include scheduled real power of all generators (except swing generator *TG*1 connected to bus 1) and all generator bus voltages. Transformer tap settings are considered fixed at 1 p. u.

Table 1
Summary of the adapted IEEE 30-bus system under study.

Items	Quantity	Details
Buses	30	[26]
Branches	41	[26]
Thermal generators ($TG1, TG2, TG3$)	3	Buses: 1 (swing), 2 and 8
Wind generator (WG)	1	Bus: 5
Solar PV unit (SPV)	1	Bus: 11
Solar PV + small-hydro (SPH)	1	Bus: 13
Control parameters	11	Scheduled real power of 5 generators: $TG2, TG3$, WG, SPV and SPH; bus voltages of all 6 generator buses
Connected load	–	283.4 MW, 126.2 MVAr
Load bus voltage range allowed	24	[0.95–1.05] p.u.

2.1. Generation cost of thermal power units

Fuel or generation cost (in $/h) of thermal generators follows a quadratic relationship with the generated output power (in MW). The same can be expressed as [20]:

$$C_{T0}(P_{TG}) = \sum_{i=1}^{N_{TG}} a_i + b_i P_{TGi} + c_i P_{TGi}^2 \tag{1}$$

where a_i, b_i, c_i represent the cost coefficients of the i-th thermal power unit generating power P_{TGi}. Total number of thermal generators in the network is N_{TG}.

In reality, the generator cost function is not smooth because of valve point loading effect. The flow of steam to the turbine blades is controlled through different nozzle groups. Due to wire drawing effect, opening of valves suddenly increases the fuel cost. Therefore, the cost curve becomes non-smooth with many ripples [3]. The additional cost due to valve point effect is accounted for in modulus of the sinusoidal function given in equation (2) [20].

$$C_T(P_{TG}) = \sum_{i=1}^{N_{TG}} a_i + b_i P_{TGi} + c_i P_{TGi}^2 + \left| d_i \times \sin\left(e_i \times \left(P_{TGi}^{min} - P_{TGi}\right)\right)\right| \tag{2}$$

where, d_i and e_i are the coefficients for the valve-point loading effect. Minimum power of the i-th thermal unit when in operation is P_{TGi}^{min}. All cost coefficients pertaining to thermal power generators are provided in Table 2 and these are same as in Ref. [20] with exception of some realistic changes made in cost coefficient a.

2.2. Cost of uncertain and intermittent renewable sources

The difficult part in integrating the renewable sources into the grid is the intermittent and uncertain nature of these sources. Usually windfarm, solar PV farm etc. are owned by the private operator, an entity that undergoes purchase agreement of certain amount of scheduled power with grid/independent system operator (ISO). If these farms do not produce scheduled power due to non-availability or insufficiency of renewable sources, the ISO is

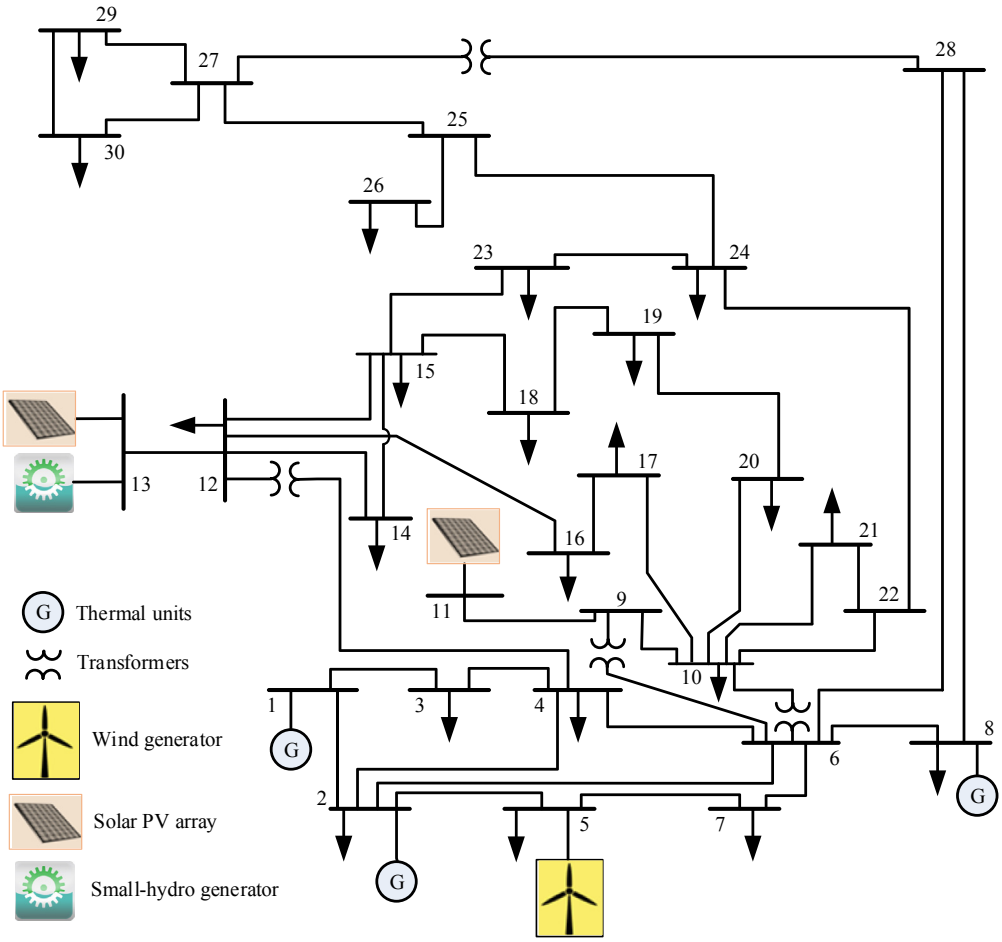

Fig. 1. Adapted IEEE 30-bus system for MOEED study with wind-solar-small hydro units.

Table 2
Cost and emission coefficients of thermal power generators.

Generator	Bus	a ($/h)	b ($/MWh)	c ($/MW^{2}h)	d ($/h)	e (rad/MW)	Φ (t/h)	Ψ (t/p.u.MWh)	ω (t/p.u.MW^{2}h)	τ (t/h)	ζ (p.u.MW^{-1})
*TG*1	1	30	2	0.00375	18	0.037	0.04091	−0.05554	0.0649	0.0002	6.667
*TG*2	2	25	1.75	0.0175	16	0.038	0.02543	−0.06047	0.05638	0.0005	3.333
*TG*3	8	20	3.25	0.00834	12	0.045	0.05326	−0.0355	0.0338	0.002	2

Note: p. u. MW calculation is on 100 MW base.

liable to mitigate the deficit amount by keeping spinning reserve if demand arises. Such scenario is termed as overestimation of renewable power and for which maintaining spinning reserve adds to the power generation cost. On contrary, situation may arise when generated power from renewable sources are more than the scheduled power. In such case of underestimation, the surplus power goes wasted if not utilized and ISO should bear the penalty cost. The total cost of the renewable sources thus consists of direct cost associated with scheduled power, penalty cost for underestimation and reserve cost for overestimation.

2.2.1. Direct cost of wind, solar photovoltaic and small-hydro power

Wind, solar and small-hydro power generators do not require any fossil fuel. In the case where these plants are owned by the independent system operator (ISO), the cost function may not exist unless ISO wants to assign some payback cost to the initial outlay for the plants or to assign this as a maintenance and renewal cost [27]. However, when these plants are owned by private operators, ISO needs to pay a price proportional to the scheduled power mutually contracted.

Direct cost of wind power from the windfarm as a function of scheduled power is represented as:

$$C_w(P_{ws}) = g_w P_{ws} \tag{3}$$

where, P_{ws} is the scheduled power as agreed from the wind power plant and g_w is the direct cost coefficient pertaining to the same plant.

Like wind power plant, direct cost associated with the solar PV plant is:

$$C_s(P_{ss}) = h_s P_{ss} \tag{4}$$

where, P_{ss} is the scheduled power from the solar PV plant and h_s is the direct cost coefficient of the same plant.

The third renewable plant considered in this study is a combination of solar PV and a small-hydro unit, owned by a single private operator. The direct cost coefficients of both these units are

different. However, scheduled output power agreed by ISO is a fixed amount and this power is delivered jointly by the solar PV and small-hydro unit. Output of the hydropower unit varies according to the flow rate of the river assuming constant head for run-of-river arrangement [28]. However, as capacity and variation of the small-hydro unit is insignificant compared to the requirement and load of the system, the unit is usually run flat out. Therefore, available amount (depending upon the river flow rate) of hydro power together with the output from solar PV unit constitutes the scheduled power.

Direct cost associated with the solar PV and small hydro unit is:

$$C_{sh}(P_{ssh}) = C_{sh}(P_{ssh,s} + P_{ssh,h}) = h_s P_{ssh,s} + m_h P_{ssh,h} \tag{5}$$

where, P_{ssh} is the scheduled power from the combined plant where contribution from solar PV plant is $P_{ssh,s}$ and small-hydro unit is $P_{ssh,h}$. Direct cost coefficient of solar PV unit is considered same as earlier (h_s) and that of small-hydro unit is m_h.

2.2.2. Uncertain wind power cost evaluation

As mentioned earlier, due to uncertain nature of wind energy, the windfarm may produce less than the scheduled amount. ISO needs to have adequate spinning reserve to mitigate the demand if such a situation arises. The cost of committing the reserve generating units to meet over-estimated amount is termed as reserve cost [20].

Reserve cost for the wind power plant is defined as [20]:

$$\begin{aligned} C_{Rw}(P_{ws} - P_{wav}) &= K_{Rw}(P_{ws} - P_{wav}) \\ &= K_{Rw}\int_0^{P_{ws}} (P_{ws} - p_w) f_w(p_w) dp_w \end{aligned} \tag{6}$$

where, K_{Rw} is the reserve cost coefficient for the wind power plant, P_{wav} is the actual available power from the same plant. $f_w(p_w)$ is the wind power probability density function. The method for calculation of output power probabilities at various wind speeds is discussed in section 3.

In the case of underestimation, actual available output power form the windfarm is more than the scheduled output. This power goes wasted if not possible to utilize by reducing power output from conventional generators. The penalty cost in such case is paid by the ISO.

Penalty cost for the wind power plant is given by Ref. [20]:

$$\begin{aligned} C_{Pw}(P_{wav} - P_{ws}) &= K_{Pw}(P_{wav} - P_{ws}) \\ &= K_{Pw}\int_{P_{ws}}^{P_{wr}} (p_w - P_{ws}) f_w(p_w) dp_w \end{aligned} \tag{7}$$

where, K_{Pw} is the penalty cost coefficient for the wind power plant, P_{wr} is rated power output from the plant.

2.2.3. Uncertain solar photovoltaic power cost evaluation

The approach for cost evaluation of uncertain and intermittent solar PV power is fundamentally same as wind power. However, solar radiation is well known for trailing lognormal PDF [18,29]. For mathematical convenience, reserve and penalty cost models are constructed in line with the concept presented in Refs. [20,30]. Power output calculation for the solar PV unit is performed in section 3.

Reserve cost for overestimation of the solar PV power is [20]:

$$\begin{aligned} C_{Rs}(P_{ss} - P_{sav}) &= K_{Rs}(P_{ss} - P_{sav}) \\ &= K_{Rs} * f_s(P_{sav} < P_{ss}) * [P_{ss} - E(P_{sav} < P_{ss})] \end{aligned} \tag{8}$$

where, K_{Rs} is the reserve cost coefficient associated with the solar PV plant, P_{sav} is the actual available power from the plant. The probability of occurrence of solar power shortage from the scheduled power (P_{ss}) is defined by $f_s(P_{sav} < P_{ss})$ and the expectation of solar PV power below P_{ss} is $E(P_{sav} < P_{ss})$.

On contrary to overestimation, penalty cost for underestimation of solar PV power is [20]:

$$\begin{aligned} C_{Ps}(P_{sav} - P_{ss}) &= K_{Ps}(P_{sav} - P_{ss}) \\ &= K_{Ps} * f_s(P_{sav} > P_{ss}) * [E(P_{sav} > P_{ss}) - P_{ss}] \end{aligned} \tag{9}$$

where, K_{Ps} is the penalty cost coefficient for the solar PV plant, $f_s(P_{sav} > P_{ss})$ is the probability of solar power being excess of the scheduled power (P_{ss}), $E(P_{sav} > P_{ss})$ is the expectation of solar PV power above P_{ss}.

2.2.4. Cost evaluation of uncertain combined solar photovoltaic and small-hydro power

Large hydro power plants have huge reservoirs, turning those plants into ideal sources for spinning reserve. However, the capacity being insignificant for the small hydro compared to the system generation and demand, the ISO may not be bothered about its spinning reserve capacity. In reality, private operators of small-hydro units may not qualify for any reserve or penalty payment. In our case, the 3rd generation system is a combination of a solar PV unit and a small-hydro unit. Output from the small-hydro unit depends on river flow rate which is well known for following gumbel distribution [31,32]. Stochastic power output from the combined system is computed in section 3. Now, solar PV qualifies for the reserve and penalty payment like the one discussed in section 2.2.3. As contribution of small-hydro is only about 10–20% of total contribution from the combined system, for calculation purpose we consider reserve and penalty payment for over-estimated and underestimated total amount of power out of the combined system.

Following equation (8), reserve cost for overestimation of the combined generation system power:

$$\begin{aligned} C_{Rsh}(P_{ssh} - P_{shav}) &= K_{Rsh}(P_{ssh} - P_{shav}) \\ &= K_{Rsh} * f_{sh}(P_{shav} < P_{ssh}) * [P_{ssh} - E(P_{shav} < P_{ssh})] \end{aligned} \tag{10}$$

where, K_{Rsh} is the reserve cost coefficient associated with the combined system, P_{shav} is the actual available power from the plant. The probability of occurrence of combined system power shortage from the scheduled power (P_{ssh}) is given by $f_{sh}(P_{shav} < P_{ssh})$ and the expectation of delivered power below P_{ssh} is $E(P_{shav} < P_{ssh})$.

Following equation (9), penalty cost for underestimation of the combined generation system power:

$$\begin{aligned} C_{Psh}(P_{shav} - P_{ssh}) &= K_{Psh}(P_{shav} - P_{ssh}) \\ &= K_{Psh} * f_{sh}(P_{shav} > P_{ssh}) * [E(P_{shav} > P_{ssh}) - P_{ssh}] \end{aligned} \tag{11}$$

where, K_{Psh} is the penalty cost coefficient associated with the combined system, $f_{sh}(P_{shav} > P_{ssh})$ is the probability of combined system power being excess of the scheduled power (P_{ssh}), $E(P_{shav} > P_{ssh})$ is the expectation of the combined system power above P_{ssh}.

2.3. Emission

Thermal generators run on fossil fuels emit harmful gases into the environment, while the renewable sources do not. The amount of emission of greenhouse gases such as SO_x and NO_x varies with the generated output power (in p. u. MW on 100 MW base) following equation (12). Emission in tonnes per hour (t/h) is computed by Ref. [20]:

$$\text{Emisson, } E_{Tot} = \sum_{i=1}^{N_{TG}} \left[\left(\varphi_i + \psi_i P_{TGi} + \omega_i P_{TGi}^2 \right) + \tau_i \exp(\zeta_i P_{TGi}) \right] \tag{12}$$

where, φ_i, ψ_i, ω_i, τ_i and ζ_i are all emission coefficients associated with the i-th thermal generator. These coefficients are provided in Table 2.

2.4. Objective of optimization

The objectives of EED problem are minimization of both generation cost and emission. Total cost of generation is the summation of thermal generator cost and direct, reserve and penalty costs for the renewable sources. Thus, total cost for 3 thermal units, one wind power unit, one solar PV and one combined solar PV and small-hydro unit can be represented as summation of equations 2–11:

$$\begin{aligned} C_{Tot} = {} & C_T(P_{TG}) + [C_w(P_{ws}) + C_{Rw}(P_{ws} - P_{wav}) + C_{Pw}(P_{wav} - P_{ws})] \\ & + [C_s(P_{ss}) + C_{Rs}(P_{ss} - P_{sav}) + C_{Ps}(P_{sav} - P_{ss})] + [C_{sh}(P_{ssh}) \\ & + C_{Rsh}(P_{ssh} - P_{shav}) + C_{Psh}(P_{shav} - P_{ssh})] \end{aligned} \tag{13}$$

Objectives of multiobjective optimization:

$$\text{Minimize}[C_{Tot}\ ,\ E_{Tot}] \tag{14}$$

The EED objectives are subject to many system equality and inequality constraints.

2.4.1. Equality constraints

Equality constraints are for instantaneous power balance where generated active and reactive power must be equal to the demand and losses in the network [20].

$$P_{Gi} - P_{Di} - V_i \sum_{j=1}^{NB} V_j \left[G_{ij} \cos(\delta_{ij}) + B_{ij} \sin(\delta_{ij}) \right] = 0 \ \forall \ i \in NB \tag{15}$$

$$Q_{Gi} - Q_{Di} - V_i \sum_{j=1}^{NB} V_j \left[G_{ij} \sin(\delta_{ij}) - B_{ij} \cos(\delta_{ij}) \right] = 0 \ \forall \ i \in NB \tag{16}$$

where $\delta_{ij} = \delta_i - \delta_j$, is the voltage angle difference between buses i and j. Active and reactive load demands at bus i are P_{Di} and Q_{Di} respectively, while active and reactive power generations from a source (conventional or renewable) connected at bus i are P_{Gi} and Q_{Gi} respectively. Number of buses in the network is NB. Transfer conductance between buses i and j is G_{ij} and the susceptance between the same set of buses is B_{ij}.

2.4.2. Inequality constraints

The inequality constraints for EED problem are the operational limits of all the generators, prohibited operating zones (POZs) of thermal units and security constraints on system transmission lines and buses. Equations (17)–(20) represent the active power generation limits of thermal, wind, solar PV generators and combined generation system, respectively. Equations (21)–(24) define the reactive power capabilities of the generators following same order of thermal, wind, solar and solar-small hydro units.

a Generator constraints: Operational limits

$$P_{TGi}^{min} \le P_{TGi} \le P_{TGi}^{max} \ \ \forall \ i \in N_{TG} \tag{17}$$

$$P_{\text{ws}}^{min} \le P_{ws} \le P_{\text{ws}}^{max} \tag{18}$$

$$P_{ss}^{min} \le P_{ss} \le P_{ss}^{max} \tag{19}$$

$$P_{ssh}^{min} \le P_{ssh} \le P_{ssh}^{max} \tag{20}$$

$$Q_{TGi}^{min} \le Q_{TGi} \le Q_{TGi}^{max} \ \forall \ i \in N_{TG} \tag{21}$$

$$Q_{\text{ws}}^{min} \le Q_{ws} \le Q_{\text{ws}}^{max} \tag{22}$$

$$Q_{ss}^{min} \le Q_{ss} \le Q_{ss}^{max} \tag{23}$$

$$Q_{ssh}^{min} \le Q_{ssh} \le Q_{ssh}^{max} \tag{24}$$

The cost curve of thermal generator may be discontinuous as the whole operating range is sometimes unavailable due to vibration in shaft bearing, fault in the machine or its accessories such as pumps, boilers etc. [11]. Therefore, in operational range certain zones are introduced within which the thermal generator is not allowed to operate. These zones are known as prohibited operating zones (POZs) and can simply be represented as:

b Generator constraints (POZs):

$$P_{TGi}^{minpoz,j} < \text{POZ}_{TGi}^{j} < P_{TGi}^{maxpoz,j} \tag{25}$$

where, $P_{TGi}^{minpoz,j}$ and $P_{TGi}^{maxpoz,j}$ are the lower and upper limits (in MW) of the j-th POZ of the i-th thermal generator. Network security constraints are expressed as:

c Security constraints:

$$V_{Gi}^{min} \le V_{Gi} \le V_{Gi}^{max} \ \forall \ i \in NG \tag{26}$$

$$V_{L_p}^{min} \le V_{L_p} \le V_{L_p}^{max} \ \forall \ p \in NL \tag{27}$$

$$S_{l_q} \le S_{l_q}^{max} \ \forall \ q \in nl \tag{28}$$

Equation (26) defines the voltage limits imposed on the generator buses with NG being the number of generators (including renewables) or generator buses. Equation (27) is for voltage constraint on load buses. Line capacity constraint is given in equation (28). NL and nl are the numbers of load buses and transmission lines respectively in the network. As mentioned before, most of the literature did not consider network security constraints in EED study. However, as all these variables have certain defined bounds, realistically these constraints should be considered. Further, generator ramp up and ramp down rates are not considered in present study. Static model of ED or EED is not concerned

with these rates as the study is performed for a specific interval with a definite network loading.

Among aforementioned various constraints, equality constraints of power balance are automatically satisfied with the convergence of power flow. Newton-Raphson iterative method is applied to perform power flow calculation using software tool MATPOWER [37]. Inequality constraints on control variables viz. generator active power (except swing/slack bus generator) and generator bus voltages are self-limiting. The algorithm selects a feasible value within the defined range of a control variable for an iteration during optimization process. As scheduled power from a thermal generator with POZs is a decision variable, the algorithm is not allowed to select the value of the decision parameter within the ranges of POZs. Remaining inequality constraints of system state variables such as swing generator power, reactive power of all generators, line capacities and load bus voltages necessitate proper handling technique so that the defined limits are all conformed.

Other useful network parameters of power loss (P_{loss}) and voltage deviation (VD) are calculated using equations (29) and (30) respectively. Voltage deviation is the indicator of voltage quality in the network and is formulated as the cumulative voltage deviation of all load buses in the network [38].

$$P_{loss} = \sum_{q=1}^{nl} G_{q(ij)} \left[V_i^2 + V_i^2 - 2V_iV_j\cos(\delta_{ij}) \right] \tag{29}$$

$$VD = \left(\sum_{p=1}^{NL} \left| V_{L_p} - 1 \right| \right) \tag{30}$$

where, $\delta_{ij} = \delta_i - \delta_j$, is the difference in voltage angles between bus i and bus j and $G_{q(ij)}$ is the transfer conductance of branch q connecting buses i and j.

3. Calculation of stochastic power of renewable sources

3.1. Probability distribution of renewable power sources

Weibull probability density function (PDF) is predominantly used to represent wind speed distribution [18–20]. The probability of wind speed v m/s following Weibull PDF is given by Ref. [20]:

$$f_v(v) = \left(\frac{\beta}{\alpha}\right)\left(\frac{v}{\alpha}\right)^{(\beta-1)} e^{-(v/\alpha)^{\beta}} \text{ for } 0 < v < \infty \tag{31}$$

where, α and β are the scale and shape parameters respectively for the PDF. In present study, conventional generator at bus 5 of IEEE 30-bus system is replaced with wind power from a windfarm. Selected values of Weibull scale (α) and shape (β) parameters are provided in Table 3. All PDF parameter values are realistically chosen considering installed capacity of the power generating sources; with many of these parameters being almost same as in Ref. [20]. Fig. 2 represents Weibull fitting and wind speed frequency distributions, obtained after running 8000 Monte-Carlo scenarios.

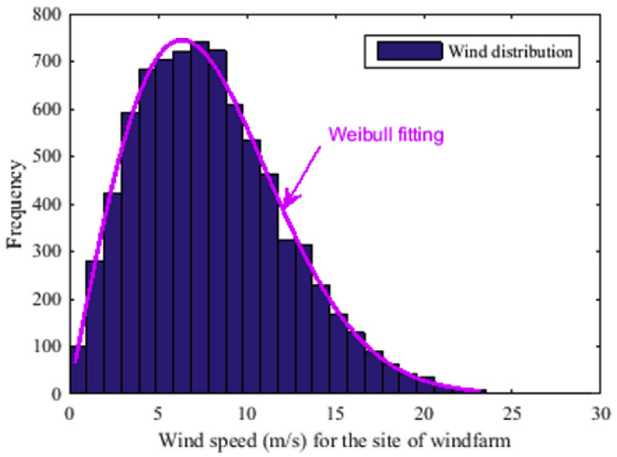

Fig. 2. Wind speed (v) distribution (sample size 8000) for the windfarm connected to bus 5 ($\alpha = 9$, $\beta = 2$).

Lognormal PDF correctly represents distribution of solar irradiance (G_s) [18,29]. The probability of solar irradiance (G_s) trailing lognormal PDF with mean μ and standard deviation σ is [20]:

$$f_G(G_s) = \frac{1}{G_s\sigma\sqrt{2\pi}} \exp\left\{ \frac{-(\ln G_s - \mu)^2}{2\sigma^2} \right\} \text{ for } G_s > 0 \tag{32}$$

Conventional generator at bus 11 of IEEE 30-bus system is substituted with solar PV unit in our study. Lognormal fitting and frequency distribution of solar irradiance in Fig. 3 with certain PDF parameters are obtained after running Monte Carlo simulation with a sample size of 8000.

It is well established that river flow rate follows Gumbel

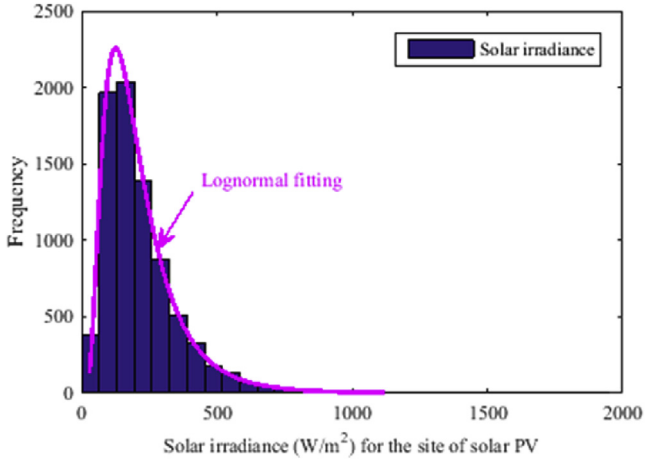

Fig. 3. Solar irradiance (G_s) distribution (sample size 8000) for solar PV at bus 11 ($\mu = 5.2$, $\sigma = 0.6$).

Table 3
PDF parameters for stochastic models of renewable sources.

Wind power plant (bus 5)			Solar PV plant (bus 11)		Combined solar PV + small-hydro (bus 13)			
No. of turbines	Total rated power,P_{wr}	Weibull PDF parameters	Rated power,P_{sr}	Lognormal PDF parameters	Solar PV rated power, P_{sr}	Lognormal PDF parameters	Small-hydro rated power, P_{hr}	Gumbel PDF parameters
25	75 MW	$\alpha = 9, \beta = 2$	50 MW	$\mu = 5.2, \sigma = 0.6$	45 MW	$\mu = 5.0, \sigma = 0.6$	5 MW	$\lambda = 15, \gamma = 1.2$

distribution [31,32], an extreme value distribution. The probability of river flow rate Q_w following Gumbel distribution with location parameter λ and scale parameter γ is written as:

$$f_Q(Q_w) = \frac{1}{\gamma}\exp\left(\frac{Q_w-\lambda}{\gamma}\right)\exp\left[-\exp\left(\frac{Q_w-\lambda}{\gamma}\right)\right] \quad (33)$$

At bus 13 of the adapted IEEE 30-bus system a small-hydro together with a solar PV unit is connected, replacing the conventional generator. Fig. 4 is for the solar irradiance distribution and lognormal fitting available for the solar PV at bus 13, while Fig. 5 is for the river flow rate frequency distribution and Gumbel fitting. Both these diagrams are generated after running 8000 Monte Carlo scenarios with selected values of PDF parameters which are provided in Table 3.

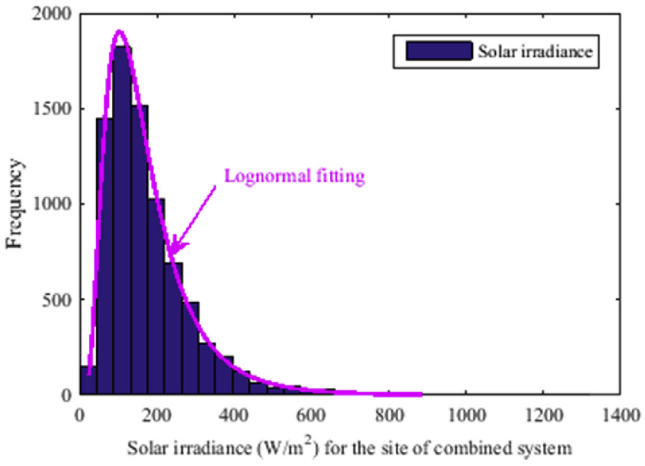

Fig. 4. Solar irradiance (G_s) distribution (sample size 8000) for solar PV at bus 13 (μ = 5.0, σ = 0.6).

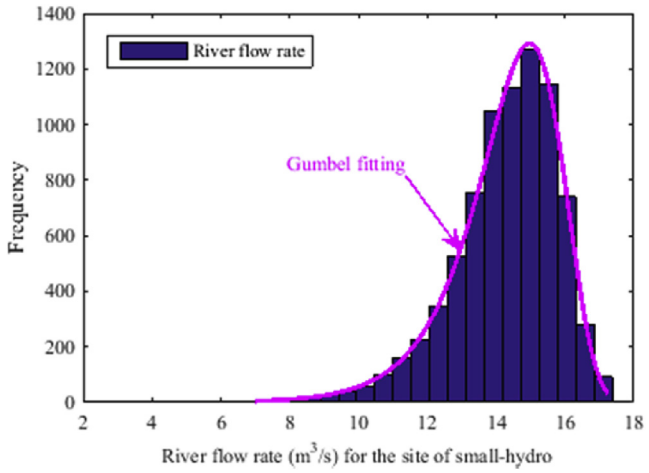

Fig. 5. River flow rate (Q_w) distribution (sample size 8000) for small-hydro at bus 13 (λ = 15, γ = 1.2).

3.2. Power models for wind, solar photovoltaic and small-hydro units

The windfarm connected to bus 5 is assumed to have all similar 25 turbines of 3 MW each; thereby totaling the farm capacity to 75 MW. Output power from a wind turbine varies according to the wind speed it encounters. The relationship between output power and wind speed (v) is expressed as [20]:

$$p_w(v) = \begin{cases} 0, & \text{for } v < v_{in} \text{ and } v > v_{out} \\ p_{wr}\left(\dfrac{v-v_{in}}{v_r-v_{in}}\right) & \text{for } v_{in} \le v \le v_r \\ p_{wr} & \text{for } v_r < v \le v_{out} \end{cases} \quad (34)$$

where, p_{wr} is the rated output power of single wind turbine. v_{in}, v_r and v_{out} are the cut-in, rated and cut-out wind speeds of the turbine, respectively. The various speed values considered in our study are v_{in} = 3 m/s, v_r = 16 m/s and v_{out} = 25 m/s, in line with the data of Enercon E82-E4 turbine.

The solar irradiance (G_s) to energy conversion for solar PV is given by Ref. [20]:

$$P_s(G_s) = \begin{cases} P_{sr}\left(\dfrac{G_s^2}{G_{std}R_c}\right) & \text{for } 0 < G_s < R_c \\ P_{sr}\left(\dfrac{G_s}{G_{std}}\right) & \text{for } G_s \ge R_c \end{cases} \quad (35)$$

where, G_{std} is the solar irradiance in standard environment set as 1000 W/m^2. R_c is a certain irradiance point set as 120 W/m^2. These data are applicable to both the solar PV plant connected to bus 11 and bus 13. P_{sr} is the rated output power of the solar PV unit.

The power output from a small-hydro unit depends upon the water flow rate (Q_w) and effective pressure head (H_w). The power output from small-hydro unit can be mathematically represented as [28]:

$$P_H(Q_w) = \eta\rho g Q_w H_w \quad (36)$$

where, η is the efficiency of turbine-generator assembly, ρ is the water density and g is the acceleration due to gravity. Numerical values of these parameters considered for the calculation of hydro power are, η = 0.85, ρ = 1000 kg/m^3, g = 9.81 m/s^2 and H_w = 25 m.

3.3. Calculation of wind power probabilities

The output power from wind turbine is discrete at certain wind speeds as can be observed from equation (34). The power output is zero when wind speed (v) is below cut-in speed (v_{in}) or above cut-out speed (v_{out}). Between rated wind speed (v_r) and cut-out speed (v_{out}), the turbine produces rated power output p_{wr}. Wind power probabilities for these discrete zones are computed by Refs. [18,20]:

$$f_w(p_w)\{p_w = 0\} = 1 - \exp\left[-\left(\frac{v_{in}}{\alpha}\right)^{\beta}\right] + \exp\left[-\left(\frac{v_{out}}{\alpha}\right)^{\beta}\right] \quad (37)$$

$$f_w(p_w)\{p_w = p_{wr}\} = \exp\left[-\left(\frac{v_r}{\alpha}\right)^{\beta}\right] - \exp\left[-\left(\frac{v_{out}}{\alpha}\right)^{\beta}\right] \quad (38)$$

The wind turbine power output is continuous between cut-in speed (v_{in}) and rated speed (v_r) of wind. The probability for the continuous region is calculated as [18,20]:

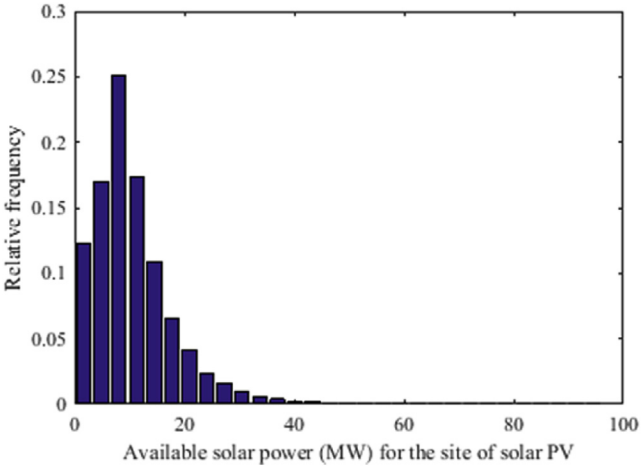

Fig. 6. Available power from solar irradiance for solar PV at bus 11.

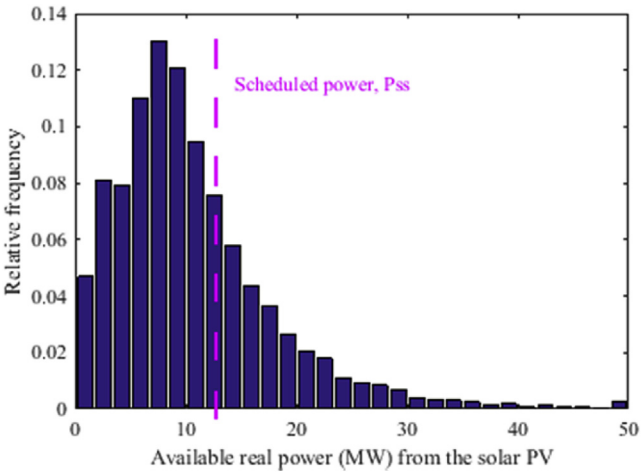

Fig. 7. Distribution of available real power (MW) from the solar PV at bus 11.

$$f_w(p_w) = \frac{\beta(v_r - v_{in})}{\alpha^{\beta} * p_{wr}} \left[v_{in} + \frac{p_w}{p_{wr}}(v_r - v_{in}) \right]^{\beta-1} \exp\left[- \left(\frac{v_{in} + \frac{p_w}{p_{wr}}(v_r - v_{in})}{\alpha} \right)^{\beta} \right] \quad (39)$$

3.4. Solar photovoltaic power over/under estimation cost calculation

Fig. 6 represents the histogram of available power from solar radiation for the site of solar PV unit connected to bus 11. It may not be possible to fully harness the available solar power as the solar PV unit and its accessories have defined capacities. Moreover, the private owner of solar PV plant may not qualify for penalty payment beyond installed (or rated) capacity of the plant. Fig. 7 provides the histogram of real power that can be delivered by the solar PV plant. The output power is capped at rated power of the unit. Scheduled power, an amount that is mutually agreed between the private operator and ISO, can be any point on horizontal axis of the diagram. The same is indicated with magenta dotted line. Now, the

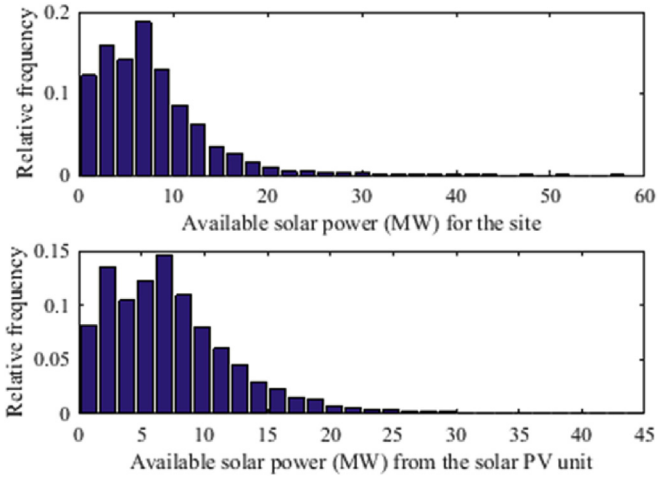

Fig. 8. Available solar power (MW) for the site and from the solar PV unit at bus 13.

cost of overestimation in equation (8) can be computed by Ref. [20]:

$$C_{Rs}(P_{ss} - P_{sav}) = K_{Rs}(P_{ss} - P_{sav}) = K_{Rs} \sum_{n=1}^{N_b^-} [P_{ss} - P_{sn-}] * f_{sn-} \quad (40)$$

where, P_{sn-} is the available power less than the scheduled power P_{ss}, on left-half plane of P_{ss} in the histogram in Fig. 7. f_{sn-} is the relative frequency of occurrence of P_{sn-}. N_b^- is the number of discrete bins on left-half of P_{ss} or simply the number of pairs (P_{sn-}, f_{sn-}) generated for the PDF. It is observed that increasing number of segments beyond a certain value does not notably impact the accuracy of results. Therefore, for practically acceptable results, a total (N_b) of 30 segments are considered for the problem under study.

For underestimation of stochastic solar power, ISO is to bear certain penalty cost. The penalty cost given in equation (9) can be calculated as [20]:

$$C_{Ps}(P_{sav} - P_{ss}) = K_{Ps}(P_{sav} - P_{ss}) = K_{Ps} \sum_{n=1}^{N_b^+} [P_{sn+} - P_{ss}] * f_{sn+} \quad (41)$$

where, P_{sn+} is the available power more than the scheduled power P_{ss}, on right-half plane of P_{ss} in the histogram in Fig. 7. f_{sn+} is the relative frequency of occurrence of P_{sn+}. N_b^+ is the number of discrete bins on right-half of P_{ss} or simply the number of pairs (P_{sn+}, f_{sn+}) generated for the PDF.

3.5. Combined solar photovoltaic and small-hydro power over/under estimation cost calculation

Available solar power for site of solar generator and from the generator connected to bus 13 are represented by the histogram in Fig. 8. Rated power of selected hydro generator unit, connected to bus 13, is larger than the available hydro power calculated from stochastic river flow rate. Fig. 9 represents the subplots of available hydro-power for the site and from the hydro unit; both subplots are same. Now, at bus 13 power from both units are summed up and the collective stochastic power output is shown in Fig. 10 histogram. Simple arithmetic point by point addition of 8000 Monte-Carlo sample points of power distributions corresponding to respective PDFs is performed to come up with the histogram in Fig. 10. As mentioned earlier, small-hydro unit may not qualify for reserve or penalty payment. However, as contribution from that unit is a small percentage of the cumulative power indicated in

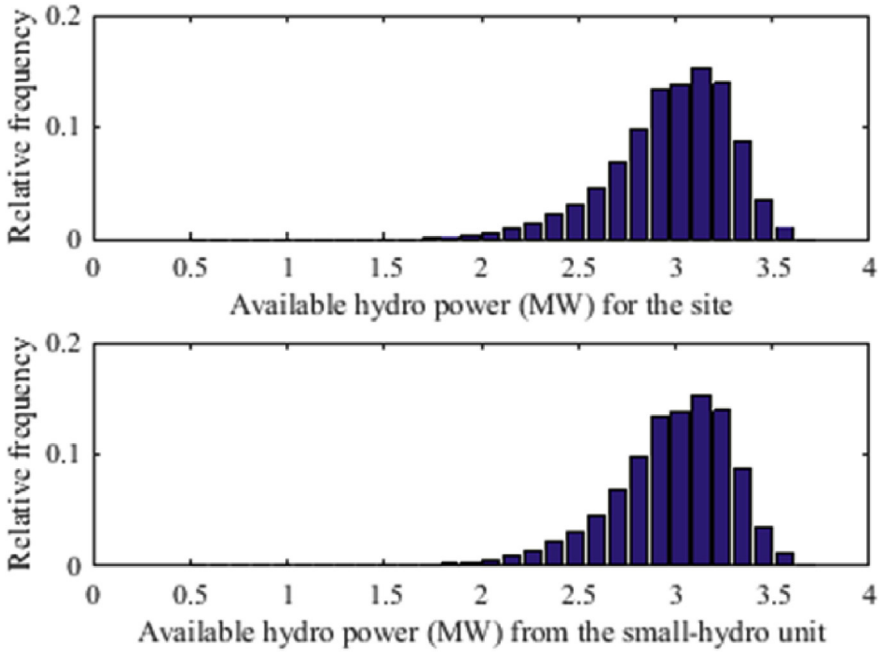

Fig. 9. Available hydro power (MW) for the site and from the small-hydro unit at bus 13.

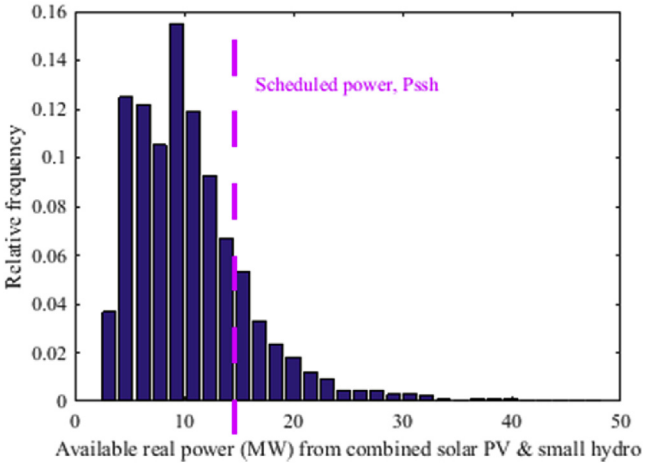

Fig. 10. Available total real power (MW) from the combined solar PV and small-hydro unit at bus 13.

Fig. 10, the reserve and penalty cost are calculated including the hydro-unit for convenience. Like equation (40), the cost of over-estimation for the combined system is:

$$C_{Rsh}(P_{ssh} - P_{shav}) = K_{Rsh}(P_{ssh} - P_{shav}) = K_{Rsh}\sum_{n=1}^{N_b^-}[P_{ssh} - P_{shn-}]^* f_{shn-} \quad (42)$$

where, P_{shn-} is the available power less than the scheduled power P_{ssh}, on left-half plane of P_{ssh} in the histogram in Fig. 10. f_{shn-} is the relative frequency of occurrence of P_{shn-}. N_b^- is the number of discrete bins on left-half of P_{ssh} or simply the number of pairs (P_{shn-}, f_{shn-}) generated for the PDF. Following equation (41), penalty cost for underestimation of the combined system is calculated as:

$$C_{Psh}(P_{shav} - P_{ssh}) = K_{Psh}(P_{shav} - P_{ssh}) = K_{Psh}\sum_{n=1}^{N_b^+}[P_{shn+} - P_{ssh}]^* f_{shn+} \quad (43)$$

where, P_{shn+} is the available power more than the scheduled power P_{ssh}, on right-half plane of P_{ssh} in the histogram in Fig. 10. f_{shn+} is the relative frequency of occurrence of P_{shn+}. N_b^+ is the number of discrete bins on right-half of P_{ssh} or simply the number of pairs (P_{shn+}, f_{shn+}) generated for the PDF.

Numerical values of direct, penalty and reserve cost coefficients for stochastic wind, solar and small-hydro power are provided in Table 4. The direct cost coefficients are decided in a way that the cost of wind energy is the highest followed by solar energy and finally the least expensive hydroelectric power [20,33]. Reserve cost coefficient for maintaining spinning reserve is higher than the respective direct cost coefficient. However, penalty cost for not using the available power is lower than the direct cost.

4. Constraint handling technique and optimization algorithms

The constraint handling technique superiority of feasible solutions (SF), multiobjective evolutionary algorithms MOEA/D and SMODE, and the integration of SF separately with the two algorithms are described in this section.

4.1. Constraint handling technique

The constraint handling technique for processing infeasible solutions was first introduced by Powell and Skolnick [34]. To handle constraints in evolutionary algorithms (EAs), Deb [24] later proposed a similar approach where he suggested to transform equality constraints into inequality constrains with the help of a tolerance parameter. In addition, all constraints were required to be normalized, else their differing numerical ranges might create bias

Table 4
Direct, penalty and reserve cost coefficients for stochastic renewable energies.

Direct cost coefficient ($/MW)			Reserve cost coefficient ($/MW)			Penalty cost coefficient ($/MW)		
Wind (bus 5)	Solar (bus 11 & 13)	Small-hydro (bus 13)	Wind (bus 5)	Solar (bus 11)	Combined solar-small hydro (bus 13)	Wind (bus 5)	Solar (bus 11)	Combined solar-small hydro (bus 13)
$g_w = 1.7$	$h_s = 1.6$	$m_h = 1.5$	$K_{Rw} = 3$	$K_{Rs} = 3$	$K_{Rsh} = 3$	$K_{Pw} = 1.4$	$K_{Ps} = 1.4$	$K_{Psh} = 1.4$

towards one or more of them. The total constraint violation is calculated as [20]:

$$\varepsilon(x) = \frac{\sum_{k=1}^{N_C} w_k T_k(x)}{\sum_{k=1}^{N_C} w_k} \tag{44}$$

where x is a solution in the search space covering both feasible and infeasible regions, $w_k(= 1/T_{k,max})$ is a weight parameter, $T_{k,max}$ is the maximum violation of constraint $T_k(x)$ obtained so far, N_C is the total number of constraints. As an obvious fact, $w_k(= 1/T_{k,max})$ varies during the evolution.

In SF, a set of rules is followed to compare two solutions x_i and x_j. x_i is considered superior to x_j when:

- x_i is feasible while x_j is infeasible
- x_i and x_j are both feasible and x_i has a smaller objective value (in a minimization problem) than x_j
- x_i and x_j are both infeasible, but x_i has a smaller overall constraint violation i.e. $\varepsilon(x_i) < \varepsilon(x_j)$.

In summary, this constraint handling technique always considers superiority of feasible solutions over infeasible ones. Two infeasible solutions are compared based on their overall constraint violations only so that the search process drives the infeasible solutions towards feasible region. Two feasible solutions are compared based on their fitness values only, thereby improving the quality of overall solution.

4.2. Multiobjective evolutionary algorithm based on decomposition

Decomposition based multiobjective evolutionary algorithm (MOEA/D) works on the principle of decomposing a multiobjective problem into several subproblems and optimizing those concurrently [21]. Multiobjective optimization problem (MOP) is defined by:

$$\text{Minimize } F(x) = \{f_1(x), f_2(x), \cdots, f_M(x)\} \tag{45}$$

where, M is the number of objectives to be optimized and for MOEED problem $M = 2$ i.e. $f_1(x) = C_{Tot}$ and $f_2(x) = E_{Tot}$ (see eq. (14)). Variable $x \in \Omega$, Ω being the decision variable space. If N is selected as population size, there will be N decision vectors $x^1, x^2, \ldots, x^N$ for the optimization problem. The EED problem for IEEE 30-bus system has 11 variables. Therefore, each decision vector x^m for $m = 1, 2, \ldots, N$ is formulated as a 11-dimensional vector. The aim of the multiobjective optimization is to find a set of *Pareto* optimal solutions that result in *Pareto* front [35] in the objective space.

4.2.1. Decomposition approach

MOEA/D decomposes the approximated *Pareto front* (PF) into many scalar optimization subproblems [36]. A few variants of MOEA/D have been developed till date. MOEA/D with dynamic resource allocation (MOEA/D-DRA) [22] is adopted for the optimization problem here. N (i.e. equals to population size) evenly spread weight vectors $\lambda^1, \lambda^2 \ldots \lambda^N$ are required to decompose the MOP. The dimension of each weight vector will be M (i.e. number of objectives) and in vector form $\lambda^m = (\lambda_1^m, \lambda_2^m, \ldots, \lambda_M^m)^T$ for $m = 1, 2, \ldots, N$. Elements of each weight vector when added up equals to 1 i.e. $\{\lambda_1^m + \lambda_2^m + \ldots + \lambda_M^m = 1\}$.

Let $z^* = (z_1^*, z_2^*, \ldots, z_M^*)^T$ is the vector that contains minimum values for the objectives. The vector is treated as the reference point and its elements are calculated as $z_i^* = \min\{f_i(x) | x \in \Omega\}$, where $i = 1, 2, \ldots, M$. The MOP after being decomposed into N subproblems, the objective function of m-th subproblem becomes:

$$g^{te}(x|\lambda^m, z^*) = \max_{1 \le i \le M} \{\lambda_i^m |f_i(x) - z_i^*|\} \tag{46}$$

z^* is all likely to be unknown beforehand and for that reason the algorithm uses the lowest values of $f_i(x)$ found so far during the search process to substitute z_i^*. MOEA/D simultaneously minimizes objective functions of all N subproblems in a single run. The optimization process of a subproblem utilizes the information mainly from its neighboring subproblems. All subproblems are treated equally and given same computational effort in MOEA/D. However, in the variant MOEA/D-DRA, based on calculated utilities of the subproblems varying computational efforts are given on different subproblems [22]. Though MOEA/D-DRA is not explicitly stated in this literature, calculated utilities of the subproblems are utilized to effect DRA methodology of the algorithm.

In MOEA/D, disparate objectives are required to be normalized, else solutions are all likely to evolve towards the objective with higher magnitude. In the problem of MOEED, numerical ranges of cost and emission are vastly different. The purpose of normalization is to maintain the range of both the objectives within 0–1. The objective function for m-th subproblem in equation (46) is to be modified as:

$$g^{te}(x|\lambda^m, z^*) = \max_{1 \le i \le M} \left\{ \lambda_i^m \left| \frac{f_i(x) - z_i^*}{z_i^{nad} - z_i^*} \right| \right\} \tag{47}$$

where, z_i^{nad} is the maximum value of $f_i(x)$ and vector $z^{nad} = (z_1^{nad}, z_2^{nad}, \ldots, z_M^{nad})^T$. Like z^*, z^{nad} is also evaluated by the algorithm during the search process using all maximum values of $f_i(x)$.

During the search process, MOEA/D with Tchebycheff approach [35] maintains:

- A population of N vectors $x^1, x^2, \ldots, x^N$
- Function values of $FV^1, FV^2, \ldots, FV^N$ where, $FV^m = \{f_1(x^m), f_2(x^m), \ldots, f_M(x^m)\}$ for $m = 1, 2, \ldots, N$.
- $z^* = (z_1^*, z_2^*, \ldots, z_M^*)^T$, where z_i^* is the minimum value found till now evaluating $f_i(x)$ for $i = 1, 2, \ldots, M$.
- $z^{nad} = (z_1^{nad}, z_2^{nad}, \ldots, z_M^{nad})^T$, where z_i^{nad} is the maximum value found thus far evaluating functions $f_i(x)$ for $i = 1, 2, \ldots, M$.
- Utility values of the subproblems, π^m for $m = 1,2, \ldots, N$.
- Current generation number *gen*.

4.2.2. Integration with constraint handling technique

MOEA/D when integrated with constraint handling technique SF, in addition to above the algorithm shall maintain:

- A population of N vectors containing calculated constraint violation corresponding to each of $x^1, x^2, \ldots, x^N$. If N_C is the total number of constraints in the optimization problem, each constraint violation vector is formulated as $CV^m = (CV_1^m, CV_2^m, \ldots, CV_{N_C}^m)$ for $m = 1, 2, \ldots, N$. The elements of the vector CV^m are same as T_k for $k = 1, 2, \ldots, N_C$ in equation (44).
- A population of N vectors containing maximum calculated constraint violation for each constraint found thus far corresponding to each index $m = 1, 2, \ldots, N$. Mathematically this can be expressed as, $CV_{max}^m = (CV_{1,max}^m, CV_{2,max}^m, \ldots, CV_{N_C,max}^m)$. Element of the vector CV_{max}^m is same as $T_{k,max}$ (where $k = 1, 2, \ldots N_C$) used to calculate w_k in equation (44).
- N values of total constraint violation, calculated with above data using equation (44), corresponding to each vector $x^1, x^2, \ldots, x^N$. We thus find, $\varepsilon(x^m)$ for $m = 1, 2, \ldots, N$ and construct constraint violation vector $ER = [\varepsilon(x^1), \varepsilon(x^2), \ldots, \varepsilon(x^N)]^T$.
- Vectors z^* and z^{nad} are replaced and updated during the search process based on the solutions obtained. Between feasible and infeasible solutions, objective values of feasible solution get preference to be suitably selected as z^* or z^{nad}. In a generation, a lower objective value can replace the respective element of z^* only if the constraint violation of the corresponding solution is less than or equal to the earlier solution. Same principle applies for update of z^{nad}. A higher objective value of a better solution in terms of lesser or equal constraint violation can replace corresponding element of z^{nad}.

4.2.3. Combined decomposition based multiobjective optimization algorithm and constraint handling technique

Input: (i) MOP (ii) Number of subproblems, N (iii) A uniform spread of N weight vectors, $\lambda^1, \lambda^2 \ldots, \lambda^N$ (iv) T: the number of the weight vectors in the neighborhood of each weight vector (v) a termination criterion, *Maxeval*.

Output: $\{x^1, x^2, \ldots, x^N\}$ and $\{f_1(x^m), f_2(x^m), \ldots f_M(x^m), \varepsilon(x^m)\}$ for $m = 1, 2, \ldots, N$.

Step 1 - Initialization: Initialize decision vectors with randomly generated solutions in the search space. Calculate total constraint violation $\varepsilon(x^m)$ for each initialized decision vector as described in 4.2.2 and set all such values as initial violation values. Initialize N uniformly spread weight vectors, z^* and z^{nad}. If no solution is feasible in initial population, both z^* and z^{nad} are initialized based on objective values of the initialized member that results in least constraint violation. Compute Euclidean distance between any two weight vectors to define T-neighbors of each weight vector. Set generation counter, $gen = 1$ and utility function value $\pi^m = 1$ for all subproblems.

Step 2 – Selecting subproblems and updating the solutions: Each subproblem is associated with a weight vector and a solution. The neighborhood is always defined by the positions of the weight vectors. The N_S neighborhood of a weight vector is the set of N_S closest weight vectors (by Euclidean distance) to it and if two weight vectors are neighbors, the respective subproblems are also neighbors. In each generation, subproblems are selected based on their utility values using 10-tournament selection method [22] and 20% of the total number of subproblems are identified in the process. The current solutions corresponding to the selected indices of subproblems are picked up in the current generation for further operation. For each selected solution x^m, MOEA/D does the following [36]:

i. Set the mating and update range P to be the T-neighborhood of x^m with a large probability δ, and the whole population otherwise.
ii. Randomly select three current solutions from P.
iii. Generate a new solution y^m by performing mutation and crossover on the selected solutions with pre-defined mutation factor F and crossover rate CR. Repair y^m if it goes outside the range. Compute objective $F(y^m)$ and total constraint violation $\varepsilon(y^m)$.
iv. If y^m yields lesser constraint violation or zero constraint violation together with better fitness value than current FV of related subproblem, replace a small number (n_r) of solutions in P by y^m.

No solution will be replaced in (iv) above if y^m produces larger constraint violation or zero constraint violation with inferior fitness value than any solution in P for its subproblem. When such a case happens, the update is deemed to be a failure, else, it is successful.

Step 3 – Stop if the termination criterion i.e. *Maxeval* (maximum number of function evaluations) is reached.

Step 4 – $gen = gen + 1$. If gen is a multiplication of 50, update utilities of all subproblems [22]. Go to Step 2.

Table 5 lists the selected parameters for the algorithm MOEA/D-SF. Flowchart in Fig. 11 gives an overview of the steps involved in algorithm MOEA/D-SF.

4.3. Summation based multiobjective differential evolution

The common approach in multiobjective differential evolution (MODE) to rank the solutions is non-dominated sorting. But the process is complex, computationally expensive and time consuming. Summation based multiobjective differential evolution (SMODE) is proposed in Ref. [23] where summation of normalized objective values is used for ranking of solutions instead of non-dominated sorting. The purpose of normalization is to bring all objective values within range [0,1] by performing simple operation as:

$$f_i^{"}(x^m) = \frac{f_i(x^m) - f_{i,min}}{f_{i,max} - f_{i,min}} \tag{48}$$

where, $f_i^{"}(x^m)$ is the normalized value of solution x^m for i-th objective, $f_{i,min}$ and $f_{i,max}$ are the minimum and maximum values for the i-th objective function. The normalized values of all objective functions for a solution are summed up, say $F^{"}(x^m) = \sum_{i=1}^{M} f_i^{"}(x^m)$ where M is the number of objective functions. For N solutions in the problem, $F^{"}$ is calculated i.e. $F^{"}(x^m)$ for $m \in \{1, 2, \ldots, N\}$. Sorting of the solutions is performed based on the resultant $F^{"}$ values. The solution that corresponds to smaller summated value is considered superior to the solution that produces larger summation of normalized objective values. To elaborate, p-th solution in the population is better than q-th solution if $F^{"}(x^p) < F^{"}(x^q)$. Post sorting of solutions, diversified selection is implemented in SMODE. During evolution, two sets of populations viz. preferential set and backup set are maintained. Members of preferential set get priority to evolve. Members of backup set are selected only if the number of individuals in preferential set is less than the population size (N). In case the number of individuals in the preferential set is larger than the population size, the required number of individuals will be randomly selected to become parents for next generation [23].

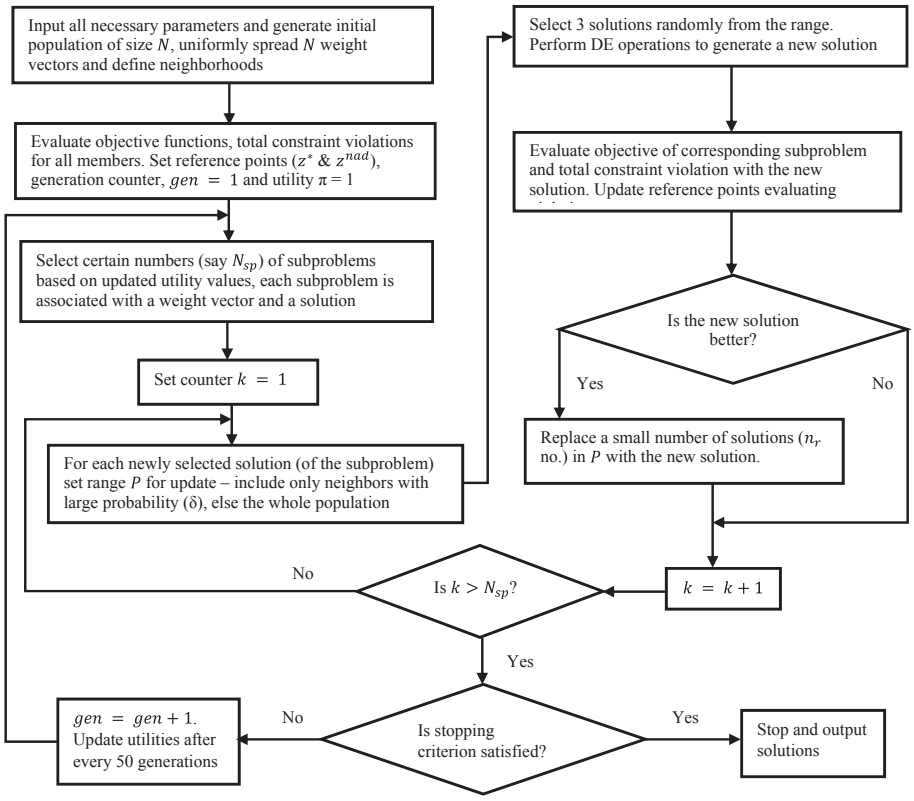

Fig. 11. Flowchart for implementation of algorithm MOEA/D-SF.

SMODE is used in conjunction with SF constraint handling technique to handle constraints of MOEED problem. The steps and approach followed are same as in Ref. [14]. Only difference is, constraint values were all summed up in Ref. [14] while we treat the constraints separately and normalize them before calculating total constraint violation using eq. (44). The operation does not notably impact final results, but it is a more appropriate method to apply SF technique. The steps of SMODE-SF can be summarized as:

Step 1 - Initialization:
- Initialize population of N individuals with uniform random distribution.
- Evaluate objective function value of each initialized individual.
- Calculate total constraint violation of each member of initial population after normalization (eq. (44)).
- Set generation counter, $gen = 1$. Define termination criteria, maximum no. of generations, *Maxgen*

Step 2 - Reproduction:
- Perform DE operations (on top N individuals) i.e. mutation and crossover with predefined scale factor (F) and crossover rate (CR) to generate N new offsprings. DE/rand/1 mutation strategy and binomial crossover are adopted [23].
- Repair the new offsprings if necessary.
- Evaluate objective functions of the newly generated offsprings.
- Calculate total constraint violation of each new offspring.
- Combine original population members with the new offsprings, i.e. total $2N$ individuals.

Step 3 - Search of feasible solutions:
- Sort the combined population in ascending order based on the values of total constraint violation.
- Identify feasible solutions i.e. solutions with zero constraint violation.
- If number of feasible solutions is less than the population size (N), **Go to Step 5.**
- If minimum N feasible individuals are present in the combined population, **Go to Step 4.**

Step 4 - Normalization and selection:
- Compute normalized objective value for each objective and each solution using eq. (48).
- Obtain summation (F'') of the normalized objective values for all solutions.
- Find Euclidean distances of all summated normalized objective values from the origin. The solution that produces total normalized objective value closest to the origin is set as the stopping point.
- Divide the objective space equally into 100 bins. Scan these bins until stopping point is included in the scanning process. In each scanned bin, the solution with lowest sum of normalized objective values is chosen to enter into the preferential set [14].
- Unselected solutions and solutions dominated by stopping point are included in backup set.

Step 5 - Termination:
- Increase generation counter by 1 i.e. $gen = gen + 1$.
- If stopping criteria *Maxgen* is reached, Stop. Else Go to Step 2.

Both the proposed algorithms are developed using MATLAB software and simulations are carried out on a computer with Intel Core i5 CPU @2.7 GHz and 4 GB RAM. The user defined input parameters for SMODE-SF are listed in Table 5. Flowchart for implementation of the algorithm SMODE-SF is provided in Fig. 12.

Table 5
MOEA/D-SF and SMODE-SF user defined input data.

MOEA/D-SF		SMODE-SF	
Parameter	Value	Parameter	Value
Population size, N	200	Population size, N	200
Number of weight vectors (equals N)	200	Mutation factor, F	0.5
Neighborhood size, T	0.15*N	Crossover rate, CR	0.9
Probability to update the neighbor (or the whole population otherwise), δ	0.9	Max no. of generations, *Maxgen*	200
Max number of positions replaced by better new solution in each subproblem at every generation, n_r	0.01*N		
Maximum number of function evaluation, *Maxeval*	100000		
Crossover rate, CR	0.9		
Mutation factor, F	0.5		

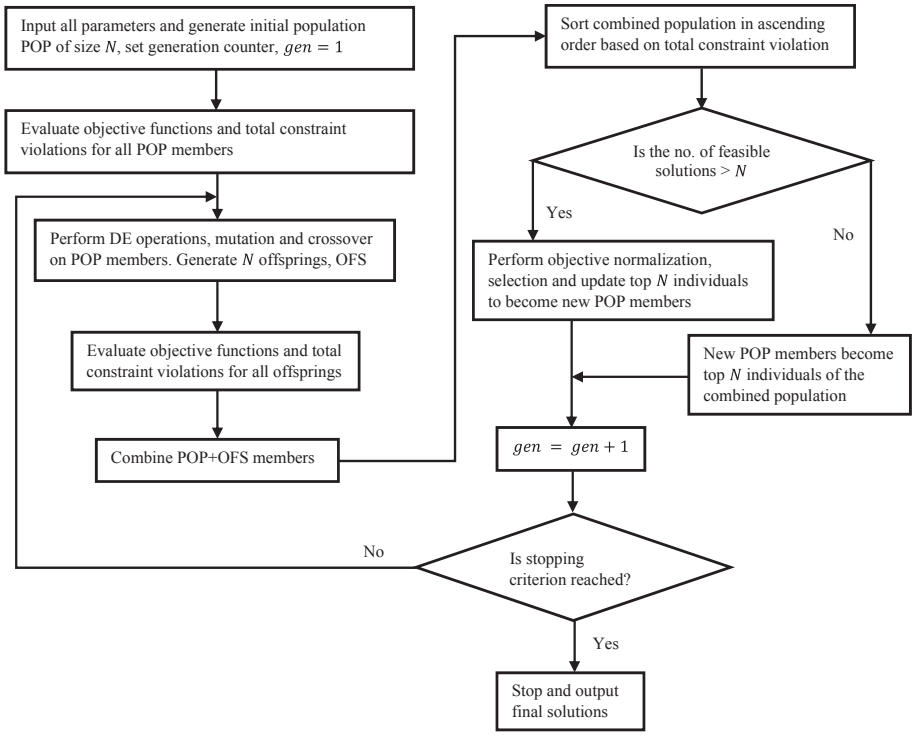

Fig. 12. Flowchart for implementation of algorithm SMODE-SF.

5. Simulation results, analysis and comparative study

In this section, simulation results after applying both the algorithms MOEA/D-SF and SMODE-SF independently on the study problem are summarized and analyzed. Hypervolume (HV) performance indicator is used to determine quality of *Pareto fronts* (PFs) attained from multiple runs of the algorithms.

5.1. Best Pareto front and best compromise solution

The study case of MOEED is run 21 times applying each algorithm. The hypervolume (HV) indicator [39,40] is calculated for the *Pareto front* (PF) of each run to evaluate its quality in terms of convergence and diversity. For multiobjective evaluation algorithms (MOEAs), the calculation of HV pertaining to a PF requires a reference point. As the two objectives of MOEED problem have different numerical ranges, the objectives are normalized to have the range between 0 and 1. The point [1,1] is considered as reference point for the two-objective optimization problem. Further, approximate HV is obtained using Monte-Carlo simulation of one million sampling points. On a given problem, among the PFs obtained from different runs, the PF with the largest HV indicator value is qualified as the best PF. The statistical details of HV indicator values with maximum, minimum, mean and standard deviation over 21 runs of each algorithm are presented in Table 6. The results are found to be consistent across all runs of an algorithm.

Table 6
Summary of hypervolume (HV) indicator values using two algorithms.

Algorithm	Max	Min	Mean	Std dev
MOEA/D-SF	0.8352	0.8337	0.8346	0.0004
SMODE-SF	0.8707	0.8635	0.8684	0.0026

Well-known fuzzy decision-making technique [9,14] is used to extract best compromise solution from the set of non-dominated solutions of best *Pareto front*. In this technique, membership function value of each objective function for a non-dominated solution is first computed as:

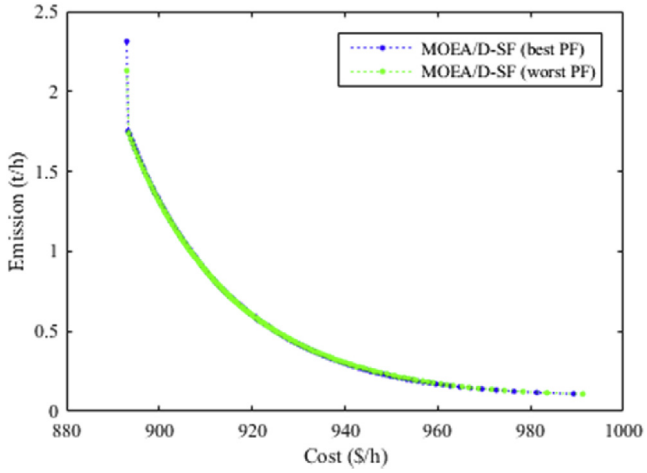

Fig. 13. Comparison of the best and the worst *Pareto fronts* of MOEA/D-SF algorithm.

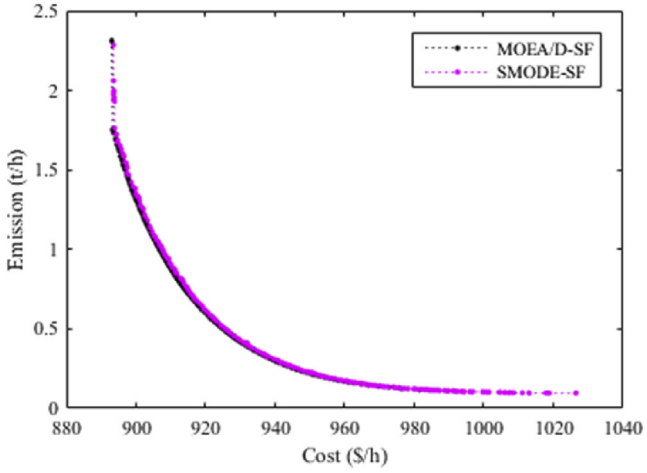

Fig. 15. Comparison of the best *Pareto fronts* of the two algorithms.

$$\xi_m^k = \begin{cases} 1 & \text{for } f_m^k \le f_m^{min} \\ \dfrac{f_m^{max} - f_m^k}{f_m^{max} - f_m^{min}} & \text{for } f_m^{min} < f_m^k < f_m^{max} \\ 0 & \text{for } f_m^k \ge f_m^{max} \end{cases} \tag{49}$$

where ξ_m^k is the membership function value of m-th objective for k-th non-dominated solution; f_m^k is the fitness value of m-th objective for k-th non-dominated solution; f_m^{min} and f_m^{max} are the minimum and maximum fitness values for the m-th objective function among all non-dominated solutions. The normalized membership function for each non-dominated solution is defined as:

$$\xi^k = \frac{\sum_{m=1}^{M} \xi_m^k}{\sum_{k=1}^{N_d} \sum_{m=1}^{M} \xi_m^k} \tag{50}$$

where, M is the number of objectives (2 here for MOEED problem) and N_d is the total number of non-dominated solutions. The solution with maximum ξ^k value is the best compromise solution.

5.2. Pareto front comparison of the two algorithms

Fig. 13 is the comparison for best and worst *Pareto fronts* (PFs) given by the algorithm MOEA/D-SF. As mentioned before, the best PF is the PF with highest HV indicator value. Curves in Fig. 14 draw same comparison of best and worst PFs for algorithm SMODE-SF. As obvious from these figures and the calculated HV indicator values that there is not much difference between best and worst PFs obtained by an algorithm. The diversity and distribution of *Pareto* optimal solutions are found slightly better in the best PFs. The difference in convergence is negligible between best and worst PFs of same algorithm. However, we are more interested in comparing results of the two algorithms. Hence, assessing the best PFs attained by the two algorithms becomes pertinent. Fig. 15 shows comparison of best *Pareto fronts* (PFs) obtained by MOEA/D-SF and SMODE-SF. As observed from the diagram, the diversity of SMODE-SF is better than MOEA/D-SF especially towards cost objective (the fact is also obvious from Figs. 13 and 14). In other words, minimum value of emission achieved by SMODE-SF is lower than what has been attained by MOEA/D-SF and this is true for all trial runs. SMODE emphasized on diversified selection process where parents for evolution are chosen according to the summation of normalized objective values and diversity with respect to each other [23].

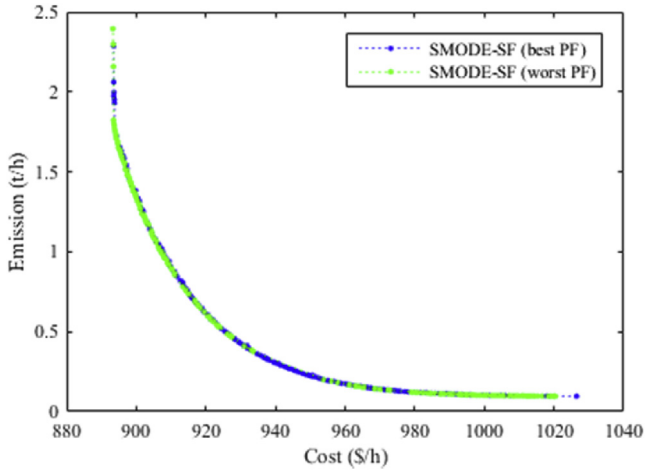

Fig. 14. Comparison of the best and the worst *Pareto fronts* of SMODE-SF algorithm.

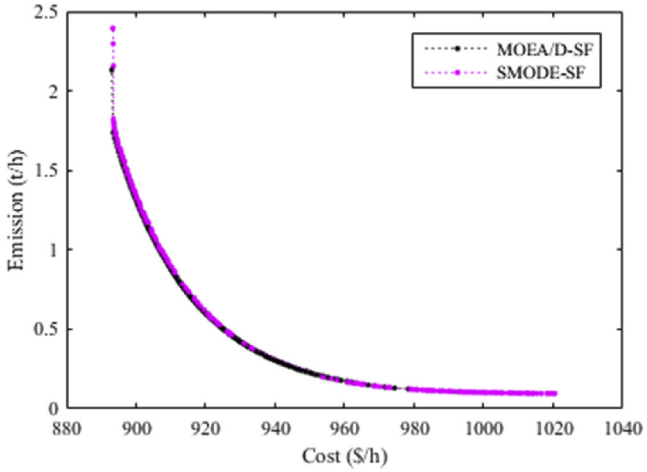

Fig. 16. Comparison of the worst *Pareto fronts* of the two algorithms.

Table 7
Detail simulation results of the optimization algorithms.

Control & state variables	Min	Max	MOEA/D-SF – Best solutions			SMODE-SF – Best solutions		
			Cost	Emission	Comp	Cost	Emission	Comp
P_{TG1} (MW)	50	140	139.048	60.003	117.118	139.848	50.047	111.91
P_{TG2} (MW)	20	80	53.763	65	65	55	47.535	65
POZ (of *TG2*): [30,40]; [55,65]								
P_{TG3} (MW)	10	35	11.558	34.89	18.403	10	35	23.555
P_{ws} (MW)	0	75	52.616	74.29	55.447	53.391	74.282	54.058
P_{ss} (MW)	0	50	17.593	28.529	17.649	16.818	50	18.436
P_{ssh} (MW)	0	50	15.319	23.755	15.326	14.989	29.336	15.755
V_1 (p.u.)	0.95	1.10	1.0785	1.0545	1.076	1.0823	1.0738	1.0761
V_2 (p.u.)	0.95	1.10	1.0644	1.0465	1.0648	1.0672	1.0596	1.0662
V_5 (p.u.)	0.95	1.10	1.0436	1.0277	1.0444	1.0406	1.0393	1.0362
V_8 (p.u.)	0.95	1.10	1.0398	1.0232	1.0402	1.0345	1.0196	1.0362
V_{11} (p.u.)	0.95	1.10	1.0876	1.0619	1.0878	1.0743	1.0576	1.0778
V_{13} (p.u.)	0.95	1.10	1.0622	1.0457	1.0602	1.0668	1.0481	1.0432
Q_{TG1} (MVAr)	−50	140	2.736	8.771	2.128	7.191	28.944	2.788
Q_{TG2} (MVAr)	−20	60	21.153	19.405	21.41	27.547	21.749	34.504
Q_{TG3} (MVAr)	−15	40	39.396	31.835	37.727	33.207	9.1	36.169
Q_{ws} (MVAr)	−30	35	27.549	22.165	27.102	24.238	25.342	20.376
Q_{ss} (MVAr)	−20	25	24.836	22.017	24.911	20.801	21.241	23.41
Q_{ssh} (MVAr)	−20	25	21.071	21.514	20.328	24.052	20.95	15.62
Total cost ($/h)			**892.954**	994.342	**919.040**	**893.314**	1020.490	**927.049**
Emission (t/h)			2.2772	**0.1052**	**0.6221**	2.3950	**0.0959**	**0.4721**
P_{loss} (MW)			6.4975	3.0671	5.5429	6.6453	2.7999	5.3148
VD (p.u.)			0.4567	0.4542	0.4530	0.4369	0.468	0.4215
$P_{ssh,h}$ (MW)			3.50	3.135	3.50	3.163	3.183	3.296

Further, two sets of populations are maintained throughout where first set of population members with lower normalized objective values in gridded objective space is given preference over other for evolution. These additional measures augur well to maintain diversity for the real-world problem such as EED. Authors in Ref. [14] also highlighted several cases where superior diversity of SMODE was established over non-dominated sorting genetic algorithm-II (NSGA-II). In terms of convergence, MOEA/D-SF is marginally better than SMODE-SF as PF of the former dominates some non-dominated solutions of the latter as observed in the diagram. In addition, distribution of solutions across PFs of MOEA/D-SF is more even as the algorithm works on the principle of uniform distribution of weight vectors [21]. Contrary to best PF, worst PF is the PF with least HV indicator value. Fig. 16 compares the worst PFs of both the algorithms for the stated problem. As in the case of best PFs' comparison, diversity of Pareto optimal solutions is found better in SMODE-SF than in MOEA/D-SF. On the other hand, uniformity in distribution of solutions and convergence are superior in MOEA/D-SF. The effectiveness of MOEA/D in generating uniform PF is also evident from the results of several case studies of other real-world problems in power domain [41,42].

5.3. Detail simulation results of the two algorithms

Table 7 presents detail simulation results alongwith control variable settings using both the algorithms, MOEA/D-SF and SMODE-SF, for best individual objectives and best compromise solutions. Best individual objective (cost or emission) is picked up from one of the 21 runs that gives best value for the respective objective. Best compromise solution is extracted from the best *Pareto front* with largest HV value among all the runs of an algorithm. Control variables are all the generator active power (except slack generator P_{TG1} connected to bus 1) and generator bus voltages. P_{ws}, P_{ss} and P_{ssh} are the scheduled power from wind, solar and combined solar-hydro units respectively. The allowable ranges of control variables are almost same as in Ref. [20]. However, discontinuity in the generator cost curve is created by introducing POZs for thermal generator *TG2* connected to bus 2. The two POZs are within ranges [30,40] MW and [55,65] MW. In addition, range of ratings for combined solar and small-hydro unit connected to bus 13 is judiciously selected based on rated power of both solar PV and small-hydro units. Active power of slack generator and reactive power of all generators are the state or dependent variables of the network. In the optimization problem, these are treated as constraints which must be satisfied by the algorithm. The wind and solar generators are considered to be capable of absorbing reactive power (negative MVAr) of about 0.4 p. u. and delivering reactive power (positive MVAr) of about 0.5 p. u. of rated capacity in line with the justification provided in Ref. [20]. Alongwith objective function values, Table 7 also includes calculated parameters of system loss using eq. (29) and cumulative voltage drop of load buses using eq. (30). The parameter $P_{ssh,h}$ (included in P_{ssh}) in the last row of the table signifies contribution from small-hydro unit. The amount of power from this unit does not follow any pattern with regard to the optimization objectives because the values of combined power from solar and small-hydro unit are obtained by simple pointwise summation of all Monte-Carlo simulation points generated independently for both the stochastic sources.

The best cost objective values achieved by both the algorithms among all trial runs are almost same and settings of corresponding control variables are also comparable. MOEA/D-SF realizes marginally lower minimum cost value, while SMODE-SF attains lesser emission value. This is to do with the well-diverse PF obtained by SMODE-SF for the highly non-linear optimization problem. In comparison of minimum emission values, the emission amount in SMODE-SF is found to be lower than MOEA/D-SF as in control variable settings 27 MW lesser loading is observed on thermal generators. Transfer of this load to renewable sources reduces the emission in the case of SMODE-SF, however, the generation cost is increased due to escalation of reserve cost linked to the higher scheduled power from renewable sources. The best compromise solutions of the two algorithms do not dominate each other on all objectives. MOEA/D-SF proposed solution is lower on cost, while the solution suggested by SMODE-SF has smaller emission value. So, it's upto the user to select based on the importance exercised on an objective. The selected compromise

solution can be any one of the two or a new solution out of many non-dominated points.

5.4. Satisfying system constraints

A very important aspect of constrained optimization problem is complying with system constraints. Non-linear constraint even in a single objective non-convex problem is a difficult proposition to deal with. For multiobjective problem such as the EED with stochastic renewable power, the situation is far more complex as the *Pareto front* (PF) involves numerous solutions which must be feasible. EED problem in many literature did not consider network security or generator reactive power constraint. Except ref. [14], either penalty function or straight disposal of infeasible solutions are some of the common methods used in literature. Here in this subsection we verify conformance to network constraints with the application of proper constraint handling technique, superiority of feasible solutions (SF) for multiobjective evolutionary algorithms. The *Pareto front* (PF) obtained from each trial run has 200 (population size) non-dominated solutions and all solutions proposed by both the algorithms are feasible. While it is not practical to validate all solutions here, we carefully select some solutions of certain trial runs and check statuses of critical constraints. The critical constraints are reactive power of generators and load bus voltages. The allowable range of load bus voltage is narrow and in many situations generators are found to be operating near to the limits as can be seen from some of the solutions in Table 7. The worst cumulative voltage-drop (*VD* in eq. (30)) among all trial runs with each algorithm is picked up and load bus voltage profile is studied for that *VD*. It is presumed that if for worst (maximum) *VD* value (and the corresponding solution) voltages of all load buses satisfy the bounds, the voltage constraint will be satisfied for other solutions with lower *VD* values. Again, for generator reactive power capability, the solutions listed in Table 7 show the compliance with the constraint. Additionally, we picked up the best PF of each algorithm and study the extreme solutions that effect minimum cost and minimum emission values.

Table 8 lists the settings of all variables for solutions resulting best cost and best emission of best PFs of the two algorithms. Fig. 17

Table 8
Settings of variables for best individual objectives of best PFs.

Control & state variables	MOEA/D-SF – Best PF		SMODE-SF – Best PF	
	Best cost	Best emission	Best cost	Best emission
P_{TG1} (MW)	139.297	62.28	139.112	50.072
P_{TG2} (MW)	55	70.051	55	52.627
P_{TG3} (MW)	10.622	35	10	34.919
P_{ws} (MW)	52.38	68.682	53.714	71.168
P_{ss} (MW)	17.348	31.034	16.167	29.555
P_{ssh} (MW)	15.328	19.509	16.057	48.254
V_1 (p.u.)	1.0806	1.069	1.0825	1.0732
V_2 (p.u.)	1.0659	1.0653	1.0646	1.0572
V_5 (p.u.)	1.0384	1.0473	1.0387	1.0076
V_8 (p.u.)	1.0376	1.042	1.0316	1.0302
V_{11} (p.u.)	1.0866	1.0681	1.0696	1.0691
V_{13} (p.u.)	1.0615	1.0582	1.0633	1.016
Q_{TG1} (MVAr)	5.317	−0.89	13.849	32.209
Q_{TG2} (MVAr)	26.047	27.845	21.72	29.609
Q_{TG3} (MVAr)	37.51	34.543	32.692	36.783
Q_{ws} (MVAr)	22.139	25.022	24.92	−5.19
Q_{ss} (MVAr)	24.903	18.508	20.113	24.951
Q_{ssh} (MVAr)	21.131	20.416	23.7	8.624
Total cost ($/h)	**893.003**	989.276	**893.503**	1018.786
Emission (t/h)	2.3134	**0.1091**	2.2868	**0.0961**
P_{loss} (MW)	6.5753	3.155	6.6492	3.1945
VD (p.u.)	0.4464	0.4382	0.4304	0.5388
$P_{ssh,h}$ (MW)	3.50	3.20	3.131	3.254

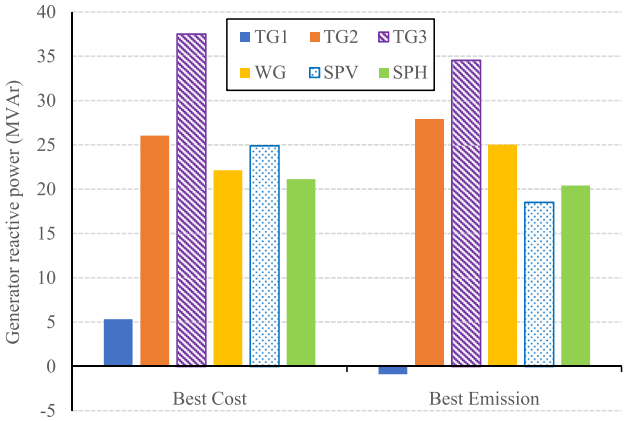

Fig. 17. Generator reactive power schedule for best objectives of the best PF using MOEA/D-SF.

Fig. 18. Generator reactive power schedule for best objectives of the best PF using SMODE-SF.

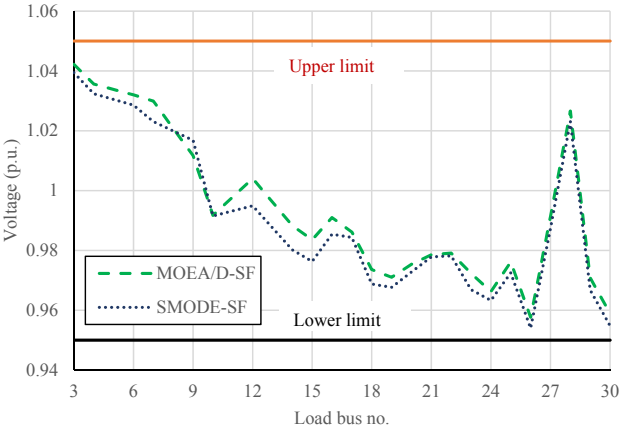

Fig. 19. Load bus voltage profiles for worst *VD* values using the two algorithms.

indicates reactive power schedule from all the generators for solutions pertaining to the best individual objective values of best PF using MOEA/D-SF. Fig. 18 describes the same schedule for solutions obtained with SMODE-SF. Looking at the diagrams and the reactive power limits provided in Table 7, it is obvious that many generators operate near to the limits of their reactive power capabilities. Therefore, caution must be exercised in satisfying this critical

constraint on generator reactive power. A proper constraint handling technique such as SF helps to select optimal settings of network control parameters so that the system can operate near to the limits without any violation. Another important observation specifically from the bar chart in Fig. 18 (i.e. reactive power schedule in Table 8 for SMODE-SF) and reactive power schedule in Table 7 for SMODE-SF is the high non-linearity of EED problem. Best emission value in Table 8 (i.e. 0.0961 t/h) of best PF obtained using SMODE-SF is almost equal to the best emission value listed in Table 7 (i.e. 0.0959 t/h) across all trial runs of the algorithm. However, the control parameter settings in both the cases are very much different. Precisely for that reason, the generator reactive power schedule in Fig. 18 (and Table 8) is totally different from the reactive power schedule in Table 7.

Each profile in Fig. 19 signifies load bus voltage profile for worst *VD* value among the *VD* values resulting from all non-dominated solutions across all trial runs using one of the two algorithms. The worst *VD* reported by MOEA/D-SF is 0.5704 p. u. while that by SMODE-SF is 0.6201 p. u. The difference is due to higher diversity of SMODE-SF helping the algorithm to attain larger extreme cost objective or smaller extreme emission objective. Analysis of the voltage profiles reveals that the operating voltages of some buses are close to the limits (either upper or lower). This fact again reiterates the effectiveness and usefulness of a suitable constraint handling technique for the evolutionary algorithms. The combination of an evolutionary algorithm (EA) and a proper constraint handling technique (such as SF) can systematically guide the search process of EA towards global feasible optima.

6. Conclusion

This paper proposes a method for finding *Pareto* optimal solutions of multiobjective economic-environmental power dispatch (MOEED) problem incorporating stochastic wind, solar and small-hydro power. In the context of current trends in energy sector and environmental regulation, such study becomes more relevant as it considers the clean and replenishable energy sources. Stochastic natures of all the renewable sources considered in this work are modelled using appropriate probability density functions (PDFs). Discontinuity in generator cost function in the form of prohibited operating zones (POZs) is also included in the model of a selected thermal generator. Multiobjective evolutionary algorithms MOEA/D and SMODE are applied to solve the multimodal, non-linear and non-convex MOEED problem. A suitable constraint handling technique, superiority of feasible solutions (SF), has been effectively integrated with the multiobjective algorithms originally developed for unconstrained optimization problem. System constraints including network security constraints are all duly satisfied with the aid of the appropriate constraint handling technique. Detail analysis of *Pareto front* with hypervolume (HV) indicator and a comparative study of the results obtained from several trials of the algorithms MOEA/D-SF and SMODE-SF are carried out. Results show that SMODE-SF outperforms MOEA/D-SF in terms of achieving diversity, though convergence of the latter is marginally better than the former. The proposed formulation on EED can further be studied using other well-known algorithms like multi-objective particle swarm optimization (MOPSO), multiobjective genetic algorithm (MOGA), non-dominated sorting genetic algorithm II (NSGA-II) etc. together with appropriate constraint handling techniques. Also, dynamic economic-environmental dispatch (DEED) problem with consideration of generator ramping rate and variation in load demands over a time-period incorporating stochastic natures of all the renewable sources and all network constraints remains a topic for future study.

Acknowledgement

This project is funded by the National Research Foundation Singapore under its Campus for Research Excellence and Technological Enterprise (CREATE) program.

References

[1] Adarsh BR, Raghunathan T, Jayabarathi T, Yang XS. Economic dispatch using chaotic bat algorithm. Energy 2016;96:666–75.
[2] Jayabarathi T, Raghunathan T, Adarsh BR, Suganthan PN. Economic dispatch using hybrid grey wolf optimizer. Energy 2016;111:630–41.
[3] Meng Anbo, Li Jinbei, Yin Hao. An efficient crisscross optimization solution to large-scale non-convex economic load dispatch with multiple fuel types and valve-point effects. Energy 2016;113:1147–61.
[4] Modiri-Delshad M, Kaboli SHA, Taslimi-Renani E, Rahim NA. Backtracking search algorithm for solving economic dispatch problems with valve-point effects and multiple fuel options. Energy 2016;116:637–49.
[5] Secui, Calin Dinu. A new modified artificial bee colony algorithm for the economic dispatch problem. Energy Convers Manag 2015;89:43–62.
[6] Gjorgiev Blaže, Marko Čepin. A multi-objective optimization based solution for the combined economic-environmental power dispatch problem. Eng Appl Artif Intell 2013;26.1:417–29.
[7] Zhang Yong, Gong Dun-Wei, Ding Zhonghai. A bare-bones multi-objective particle swarm optimization algorithm for environmental/economic dispatch. Inf Sci 2012;192:213–27.
[8] Rao B, Srinivasa, Vaisakh K. Multi-objective adaptive Clonal selection algorithm for solving environmental/economic dispatch and OPF problems with load uncertainty. Int J Electr Power Energy Syst 2013;53:390–408.
[9] Mondal Soumitra, Bhattacharya Aniruddha, Halder nee Dey Sunita. Multi-objective economic emission load dispatch solution using gravitational search algorithm and considering wind power penetration. Int J Electr Power Energy Syst 2013;44.1:282–92.
[10] Yao F, Dong ZY, Meng K, Xu Z, Iu HHC, Wong KP. Quantum-inspired particle swarm optimization for power system operations considering wind power uncertainty and carbon tax in Australia. IEEE Trans Ind Inf 2012;8(4):880–8.
[11] Jadhav HT, Roy Ranjit. Gbest guided artificial bee colony algorithm for environmental/economic dispatch considering wind power. Expert Syst Appl 2013;40.16:6385–99.
[12] Abul'Wafa Ahmed R. Optimization of economic/emission load dispatch for hybrid generating systems using controlled Elitist NSGA-II. Elec Power Syst Res 2013;105:142–51.
[13] Ghasemi A, Gheydi M, Golkar MJ, Eslami M. Modeling of Wind/Environment/Economic Dispatch in power system and solving via an online learning meta-heuristic method. Appl Soft Comput 2016;43:454–68.
[14] Qu BY, Liang JJ, Zhu YS, Wang ZY, Suganthan PN. Economic emission dispatch problems with stochastic wind power using summation based multi-objective evolutionary algorithm. Inf Sci 2016;351:48–66.
[15] Zhu Yongsheng, Wang Jie, Qu Boyang. Multi-objective economic emission dispatch considering wind power using evolutionary algorithm based on decomposition. Int J Electr Power Energy Syst 2014;63:434–45.
[16] Azizipanah-Abarghooee R, Niknam T, Roosta A, Malekpour AR, Zare M. Probabilistic multiobjective wind-thermal economic emission dispatch based on point estimated method. Energy 2012;37(1):322–35.
[17] Khan NA, Awan AB, Mahmood A, Member IEEE, Razzaq S, Zafar A, Sidhu GAS. Combined emission economic dispatch of power system including solar photo voltaic generation. Energy Convers Manag 2015;92:82–91.
[18] Reddy S Surender, Bijwe PR, Abhyankar Abhijit R. Real-time economic dispatch considering renewable power generation variability and uncertainty over scheduling period. IEEE Sys. j. 2015;9.4:1440–51.
[19] Reddy S, Surender. Optimal scheduling of thermal-wind-solar power system with storage. Renew Energy 2017;101:1357–68.
[20] Biswas Partha P, Suganthan PN, Amaratunga GA. Optimal power flow solutions incorporating stochastic wind and solar power. Energy Convers Manag 2017;148:1194–207.
[21] Zhang Qingfu, Li Hui. MOEA/D: a multiobjective evolutionary algorithm based on decomposition. IEEE Trans Evol Comput 2007;11.6:712–31.
[22] Zhang Qingfu, Liu Wudong, Li Hui. The performance of a new version of MOEA/D on CEC09 unconstrained MOP test instances. IEEE Congress Evolut. Comput. 2009;1.
[23] Qu Bo-Yang, Suganthan PN. Multi-objective evolutionary algorithms based on the summation of normalized objectives and diversified selection. Inf Sci 2010;180.17:3170–81.
[24] Deb K. An efficient constraint handling method for genetic algorithms. Comput Meth Appl Mech Eng 2000;186:311–38.
[25] Paish Oliver. Small hydro power: technology and current status. Renew Sustain Energy Rev 2002;6.6:537–56.
[26] Alsac O, Stott B. Optimal load flow with steady-state security. IEEE Trans Power Apparatus Syst 1974;3:745–51.
[27] Chen Chun-Lung, Lee Tsung-Ying, Rong-Mow Jan. Optimal wind-thermal coordination dispatch in isolated power systems with large integration of wind capacity. Energy Convers Manag 2006;47.18:3456–72.

[28] Wijesinghe Anuradha, Lai Loi Lei. Small hydro power plant analysis and development." electric utility deregulation and restructuring and power technologies (DRPT). In: 2011 4th international conference on. IEEE; 2011.
[29] Chang, Pau Tian. Investigation on frequency distribution of global radiation using different probability density functions. Int J Appl Sci Eng 2010;8.2: 99–107.
[30] Shi L, Wang C, Yao L, Ni Y, Bazargan M. Optimal power flow solution incorporating wind power. IEEE Sys J 2012;6(2):233–41.
[31] Mujere Never. Flood frequency analysis using the Gumbel distribution. Int J Comput Sci Eng 2011;3.7:2774–8.
[32] Cabus Pieter. River flow prediction through rainfall–runoff modelling with a probability-distributed model (PDM) in Flanders, Belgium. Agric Water Manag 2008;95.7:859–68.
[33] Black Veatch. Cost and performance data for power generation technologies. Prep Nat Renew Energy Lab 2012.
[34] Powell David, Skolnick Michael M. Using genetic algorithms in engineering design optimization with non-linear constraints. In: Proceedings of the 5th international conference on genetic algorithms. Morgan Kaufmann Publishers Inc; 1993.
[35] Miettinen Kaisa. Nonlinear multiobjective optimization, vol. 12. Springer Science & Business Media; 2012.
[36] Zhao Shi-Zheng, Suganthan PN, Zhang Q. Decomposition-based multiobjective evolutionary algorithm with an ensemble of neighborhood sizes. IEEE Trans Evol Comput 2012;16.3:442–6.
[37] R.D. Zimmerman, C.E. Murillo-Sánchez, R.J. Thomas, Matpower (Available at:) www.pserc.cornell.edu/matpower.
[38] Biswas Partha P, Suganthan PN, Mallipeddi R, Amaratunga GA. Optimal power flow solutions using differential evolution algorithm integrated with effective constraint handling techniques. Eng Appl Artif Intell 2018;68:81–100.
[39] While L, Hingston P, Barone L, Huband S. A faster algorithm for calculating hypervolume. IEEE Trans Evol Comput 2006;10(1):29–38.
[40] Bringmann Karl, Friedrich Tobias. Approximation quality of the hypervolume indicator. Artif Intell 2013;195:265–90.
[41] Biswas Partha P, Suganthan PN, Amaratunga GA. "Decomposition based multi-objective evolutionary algorithm for windfarm layout optimization. Renew Energy 2018;115:326–37.
[42] Biswas Partha P, Mallipeddi R, Suganthan PN, Amaratunga GA. A multiobjective approach for optimal placement and sizing of distributed generators and capacitors in distribution network. Appl Soft Comput 2017;60: 268–80.